Dynamical Effects of Non-Linearities and Time-Varying Gain Modulation in Neurally Plausible Network Models of Perceptual Decision-Making

By

Ritwik K. Niyogi

Submitted in partial fulfillment of the requirements
for departmental honors in Mathematics
Dickinson College, 2008-2009

Dr. KongFatt Wong-Lin, Advisor
Prof John MacCormick, Reader
Prof Jeffrey S. Forrester, Reader
Prof Lars Q. English, Reader

May 10, 2009

The Department of Mathematics and Computer Science at Dickinson College hereby accepts this senior honors thesis by Ritwik K. Niyogi, and awards departmental honors in Mathematics.

KongFatt Wong-Lin (Advisor) Date

John MacCormick (Reader) Date

Jeffrey S. Forrester (Reader) Date

David S. Richeson (Department chairperson) Date

Department of Mathematics and Computer Science
Dickinson College

May 10, 2009

Abstract

Dynamical Effects of Non-Linearities and Time-Varying Gain Modulation in Neurally Plausible Network Models of Perceptual Decision-Making

by
Ritwik K. Niyogi

Simple perceptual decision-making links sensation to action and constitutes the basis of many cognitive processes. Recent studies in neuroscience have made progress in identifying the neural systems associated with such processes. In particular, electrophysiological recordings from behaving primates have found the neuronal correlates of temporal integration of sensory information during perceptual decision-making tasks. However, less is known about how the underlying decision network operates, and how it can be adapted or modified to achieve behavioral goals.

Mathematical modeling of these decision processes seeks to provide a theoretical framework against which experimental findings can be interpreted and evaluated. We use computational and analytical techniques from dynamical systems theory to study non-linear and linearized versions of neurally plausible low-dimensional neural network models, which accumulate sensory evidence over time in order to form a categorical perceptual choice among two competing alternatives. In particular, we investigate how non-linearities in and multiplicative gain modulation of neural input-output (transfer) functions (e.g. due to attentional processes) can affect the dynamics of the decision network. Our work extends previous modeling efforts and generates predictions about how the stability and behavior of the decision network depend critically on stimulus parameters. In addition it predicts that modulation of both excitatory and inhibitory cells may be involved during temporal integration. We show how dynamic gain modulation over time can affect the temporal dynamics of the decision network, and thus enable flexible decision-making.

Acknowledgements

I thank my Mathematics Honors research supervisor, Dr. KongFatt Wong-Lin, for his proactive guidance, encouragement and his continuous dedication to persevering with me on this research project. I am grateful to him for agreeing to supervise my Honors research offsite from Princeton University. I am deeply grateful to Prof Philip J. Holmes, my mentor at Princeton University, who introduced me to the concepts and methods used in dynamical systems and under whose supervision I conducted inital parts of this research. I also thank Prof John MacCormick for advising my thesis onsite and his insightful comments on previous drafts of this thesis. Many thanks to Prof Jeffrey Forrester for encouraging me to proceed with this research and urging me to continue with it. My sincerest thanks to the several scientists to whom I presented this work and who critiqued our ideas and results.

I am indebted to Prof Lars English, for directing me towards the study of non-linear phenomena early on in my College career, and for his emphatic statement "The future is inter-disciplinary", as he encouraged me to amalgamate my diverse intellectual background and interests. I remain eternally grateful to Prof Jay McClelland, my mentor at Stanford University, who enticed me to the field of computational cognitive neuroscience and encouraged me to persist and persevere in it. I thank him for his direct guidance of my research on the neurodynamics of decision-making that I conducted under his supervision at Stanford University, and for exposing me to the work of future mentors such as Prof Holmes and Dr. Wong-Lin. I also thank Prof Anita Mareno, for instructing me on my independent research course, studying the applications of differential equations in theoretical neuroscience. Much of what I learned from that course enabled me to understand and appreciate the type of modeling work I pursue in this thesis. I am grateful to Prof Anthony Pires for facilitating the Dickinson College Library's purchase of relevant books in theoretical neuroscience for my perusal.

I am obliged to Prof Nancy Baxter-Hastings, my first advisor at Dickinson College for her continuous advice, guidance and encouragement throughout my undergraduate career, including the two years subsequent to her retirement. I thank her for the plans she crafted with me on shaping my future and focusing my diverging interests, since as early as my first year. I thank her and the Mathematics department for granting me the liberty to pursue my interdisciplinary interests and for facilitating the same. My research career thus far has blossomed in alignment with those early plans that Prof Hastings carved out. I thank her for her enthusiasm for both me and my work and dedicate this thesis to her.

Lastly, to the human will that strives to seek the truth and perseveres to achieve that which is oft unattempted, this honors thesis, along my honors theses for the Neuroscience and Physics majors, serves as my tribute.

I thank the Department of Mathematics and Computer Science, Dickinson College, for permitting me to proceed with this inter-institutional, inter-disciplinary research and for considering my candidacy for Honors in the Mathematics major.

Contents

1 Overview

Simple decisions form the basis of most psychological processes and behavior, from perception (was that a ball or a strike?), memory (is the count level or full?), to action (should I swing high or low?). Behavioral economics focuses on the outcomes on these decisions and not on the dynamics of the decision processes themselves. Neuroscientific studies have made progress in identifying the neural systems associated with such processes. However, less is known about precisely how they operate and how they are monitored and modified in order to achieve the goals of behavior. Mathematical modeling of these decision processes seeks to provide a theoretical framework against which experimental data can be interpreted and evaluated.

For my mathematics honors thesis, conducted during the 2008-09 academic year, I propose, analyze, and test neural network Leaky Competing Accumulator (LCA) models as well as neurally realistic models of decision-making. I use numerical simulations and analytical methods of dynamical systems theory to study these models, predict their behavior, and delineate parameter regimes that best correspond to empirical data.

In Section 3 we introduce the problem investigated. In Section 4, we describe the Two-Alternative Forced-Choice task in which a categorical decision between two alternatives must be made. We discuss the experimental findings from this task in Section 5. In order to mathematically model this experimental data and generate testable predictions, we first formulate the decision problem in Section 6. We deduce that a sequential sampling technique known as the Sequential Probability Ratio Test is the optimal decision-maker and describe how this can be translated into the continuous Drift Diffusion Model in Section 7. We then explore a two dimensional abstract, neural network model called the Leaky Competing Accumulator model of perceptual decision-making in Section 8. Specifically, we apply dynamical systems theory to perform mathematical analyses, exploring the model's dependence on parameters and non-linearities, and how these can enable categorical decision-making. Subsequently, we attempt to model the time-courses of neural activity, employing a reduced two-variable biophysically realistic model in Section 9. Performing similar analyses, we extend previous work and propose dynamic gain modulation, or the modificiation of the slope of an input-output function as a neurally plausible mechanism of perceptual decision-making. We discuss our results and conclude in Section 10. We begin by detailing the preliminaries necessary to fully comprehend and thereby appreciate the mathematical analyses involved in this research.

2 Preliminaries

In this section, we state the mathematical definitions and concepts that we shall employ in subsequent sections. A (continuous) **dynamical system** is represented by a system of N differential equations

$$\frac{dx_i}{dt} = F_i(x_1, x_2, \ldots, x_i, \ldots, x_N) \tag{2.1}$$

The system is linear if F_i is linear for all i, and it is non-linear otherwise. For a given set of initial conditions $x_i(0)$, we can solve the system given by Eq.(2.1). The solutions $(x_1(t), x_2(t), \ldots, x_N(t))$ then trace out the **trajectory** determining how this system evolves over time. The system is said to have reached **steady state** when

$$\frac{dx_i}{dt} = 0 \ \forall i. \tag{2.2}$$

The solution to this equation yields the **fixed points** or **steady states** of the system x_i^* such that the trajectories eventually attain these values, i.e., $x_i(t) \to x_i^*$ as $t \to \infty$. We specifically focus on 1-dimensional ($N = 1$) and 2-dimensional ($N = 2$) systems for which our research is particulary applicable. The set of trajectories $(x_1(t), x_2(t))$ for all initial conditions $x_1(0), x_2(0)$ yields the **phase-plane**. For a 2-dimensional dynamical system, the solutions to Eq. (2.2) are called the **nullclines** of the system. The point of intersection of the nullclines thus yield the fixed points.

For a 1-dimensional system, a fixed point is **stable** if small perturbations η from it decay with time. Similarly, it is **unstable** if these small perturbations increase with time. Consider a small perturbation $\eta(t) = x(t) - x^*$ from the fixed point x^*. Then, assuming F to be linear around the fixed point,

$$\dot{\eta} = \frac{d}{dt}(x - x^*) = \dot{x} \tag{2.3}$$

since $\frac{dx^*}{dt} = 0$. Thus, $\dot{\eta} = \dot{x} = F(x) = F(x^* + \eta)$. Then, using Taylor's expansion about x^*, we observe that

$$F(x^* + \eta) = F(x^*) + \eta F^{'}(x^*) + O(\eta^2) \tag{2.4}$$

Thus, neglecting terms of order 2 and higher in η, and noting that $F(x^*) = 0$, Eq. (2.3) simplifies to $\dot{\eta} \approx \eta F^{'}(x^*)$. Therefore, perturbations $\eta(t)$ grow exponential if $F^{'}(x^*) > 1$, making the fixed point unstable and decay if $F^{'}(x^*) < 1$, enabling a stable fixed point. This constitutes a **linear stability analysis**.

For a 2-dimensional system, we may linearlize around the fixed point (x_1^*, x_2^*) to perform a linear stabiility analysis and thereby determining the stability of the fixed points. Let us assume $\frac{dx_1}{dt} = F(x_1, x_2)$ and $\frac{dx_2}{dt} = G(x_1, x_2)$. Let $u = x_1 - x_1^*, v = x_2 - x_2^*$ be the components of a perturbation from the fixed point. Then,

$$\begin{aligned}
\dot{u} &= \dot{x} \\
&= F(x_1^* + u, x_2^* + v) \\
&= F(x_1^*, x_2^*) + u\frac{\partial F}{\partial x_1} + v\frac{\partial F}{\partial x_2} + O(u^2, v^2, uv) \\
&= u\frac{\partial F}{\partial x_1} + v\frac{\partial F}{\partial x_2} + O(u^2, v^2, uv), \qquad (2.5)
\end{aligned}$$

where the partial derivatives are evaluated at the fixed point. Similarly, $\dot{v} = u\frac{\partial G}{\partial x_1} + v\frac{\partial G}{\partial x_2} + O(u^2, v^2, uv)$. Since the perturbations u, v are small, we can neglect quadratic terms, i.e. $O(u^2, v^2, uv) \approx 0$. We can then write these equations in matrix form

$$\begin{pmatrix} \dot{u} \\ \\ \dot{v} \end{pmatrix} = \begin{pmatrix} \frac{\partial F(x_1^*, x_2^*)}{\partial x_1} & \frac{\partial F(x_1^*, x_2^*)}{\partial x_2} \\ \\ \frac{\partial G(x_1^*, x_2^*)}{\partial x_1} & \frac{\partial G(x_1^*, x_2^*)}{\partial x_2} \end{pmatrix} \begin{pmatrix} u \\ \\ v \end{pmatrix}. \qquad (2.6)$$

The let the Jacobian matrix be defined as

$$J(x_1^*, x_2^*) = \begin{pmatrix} \frac{\partial F(x_1^*, x_2^*)}{\partial x_1} & \frac{\partial F(x_1^*, x_2^*)}{\partial x_2} \\ \\ \frac{\partial G(x_1^*, x_2^*)}{\partial x_1} & \frac{\partial G(x_1^*, x_2^*)}{\partial x_2} \end{pmatrix} \qquad (2.7)$$

Let $\tau = \frac{\partial F(x_1^*, x_2^*)}{\partial x_1} + \frac{\partial G(x_1^*, x_2^*)}{\partial x_2}$ be the trace and Δ be the determinant of this matrix. In order to deduce close-form solutions for this equation, we find the eigenvalues Λ of the Jacobian matrix, we note that $\det(J - \Lambda I) = 0$, where I is the identity matrix. We then solve the characteristic polynomial equation

$$\Lambda^2 - \tau\Lambda + \Delta = 0, \qquad (2.8)$$

obtaining 2 eigenvalues Λ_1 and Λ_2. Then $u(t) = e^{\Lambda_1 t}$ and $v(t) = e^{\Lambda_2 t}$. If both $\Lambda_1, \Lambda_2 < 0$, then the fixed point is a **sink**. If both $\Lambda_1, \Lambda_2 > 0$, it is a **source**. If $\Lambda_1 > 0$ and $\Lambda_2 < 0$ or vice versa, then the fixed point is a **saddle**. The set of initial conditions $x_1(0), x_2(0)$ for which $(x_1(t), x_2(t)) \to (x_1^*, x_2^*)$ as $t \to \infty$ is called the **stable manifold** of the saddle. Similarly, the set of initial conditions $x_1(0), x_2(0)$ for which $(x_1(t), x_2(t)) \to (x_1^*, x_2^*)$ as $t \to -\infty$ is called the **unstable manifold** of the saddle. Thus, we note that a trajectory typically approaches the unstable manifold as $t \to \infty$. The set of initial conditions for which trajectories approach the sink (or attracting fixed point) is called the **basin of attraction** for the sink.

In order to study the dependence of the eventual behavior of system on parameters, we may vary a particular parameter and note what fixed points exist, and whether they are stable or unstable. This constitutes a **bifurcation** diagram.

3 Introduction

The ability to optimize behavior in the face of competing goals is imperative for the survival of any organism. Whereas behavioral economics has focused on optimal outcomes, understanding the dynamics and mechanisms of the decision process itself is crucial and is currently the focus of much decision-making research, both at the theoretical and experimental levels. Recording, evaluating and modeling the time-course of a decision process yields a deeper understanding of the mechanisms underlying decision making, especially when time is of essence, either because of a predetermined deadline for responding or because rapid responding is extremely profitable.

Electrophysiological recordings from the parietal cortices of awake, behaving primates has revealed the time-course of decision-making in simple, perceptual choice experiments [22, 29] . Behavioral results show robust Reaction Time (RT) distributions, which are skewed toward longer rection times. These empirical results have been approximated by mathematical models, which make three principal assumptions: (i) evidence in favor of each of the decision alternatives is accumulated over time, (ii) the stimulus is inherently noisy and the decision process is subject to random fluctuations and (iii) a decision is rendered when evidence favoring one of the alternatives sufficiently exceeds those for other alternatives [2, 33]. These models, while based on similar assumptions, vary in the degree to which they integrate evidence and approximate biological phenomena. Whereas neurally realistic models of several neurons can describe the time-courses of neuronal firing rates, obtained from electrophysiological recordings, neural-network and reduced, mean-field models can be used to propose optimal decision policies, against which behavioral data can be compared. A large amount of behavioral and electrophysiological experimental data as well as a variety of mathematical models exist for simple, Two-Alternative Forced-Choice (TAFC) tasks [17, 18, 19, 9].

4 The Two-Alternative Forced-Choice (TAFC) Task

In the TAFC task, a choice must be made between 2 alternatives, based on limited information about which one is correct (that is, which one gets rewarded). The TAFC is simple and representative of a natural decision such as inferring the direction of a stimulus motion or deciding whether to approach or avoid a stimulus. A common TAFC used in both human behavioral psychology and primate electrophysiology experiments involves subjects identifying the direction of motion of a group of coherently moving dots from a background of other, randomly moving dots, all of which are presented on a screen. The stimulus fidelity or task difficulty can be varied by altering motion strength or coherence, the fraction of coherently moving dots. Subjects may be instructed to respond at leisure (Fig. 1 A), before a deadline or immediately after a cue (Fig. 1 B). Additionally, the delay between the presentation of the dot motion stimulus and the response made, may be varied by the experimenter.

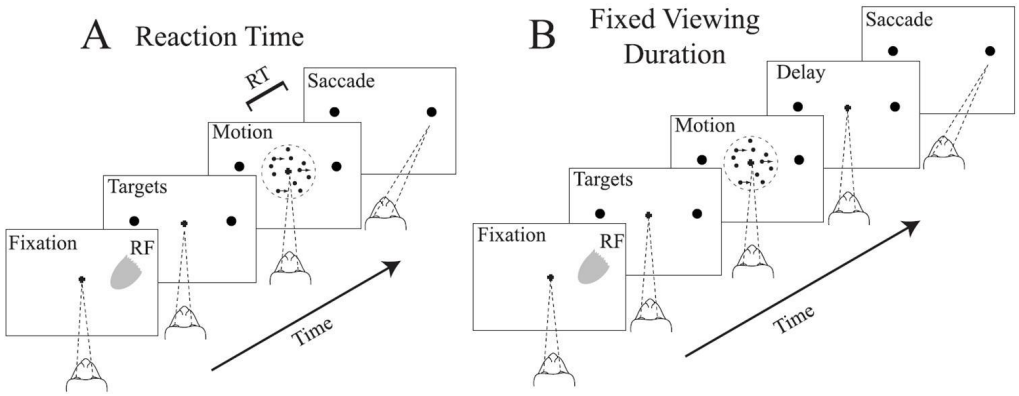

Figure 1: Two Alternative Forced-Choice Tasks. On each trial the subject is shown one of two stimuli, drawn at random. It must identify the direction (left or right) in which the majority of dots are moving. The experimenter can vary the coherence of movement (% moving left or right). Correct decisions are rewarded with either drops of juice. Primates respond by making a visual saccade towards either the left or the right. The goal of the task is to maximize reward accrued. A) Reaction Time/Free-Response task: the subject can respond at leisure. B) Fixed Viewing Duration/Interrogration Paradigm task: The subject responds at a fixed time immediately following a cue. Reproduced from [22].

5 Experimental Results

Electrophysiological recordings in the Middle Temporal (MT) and Lateral Intraparietal (LIP) cortices of awake, behaving primates (Fig. 5 A) performing the dot-motion task have revealed qualitatively distinguishable firing rate patterns of neurons in the two areas.

A stimulus comprising a majority of dots coherently moving towards the left elicited larger firing rates in neural populations in the MT (involved in the process-

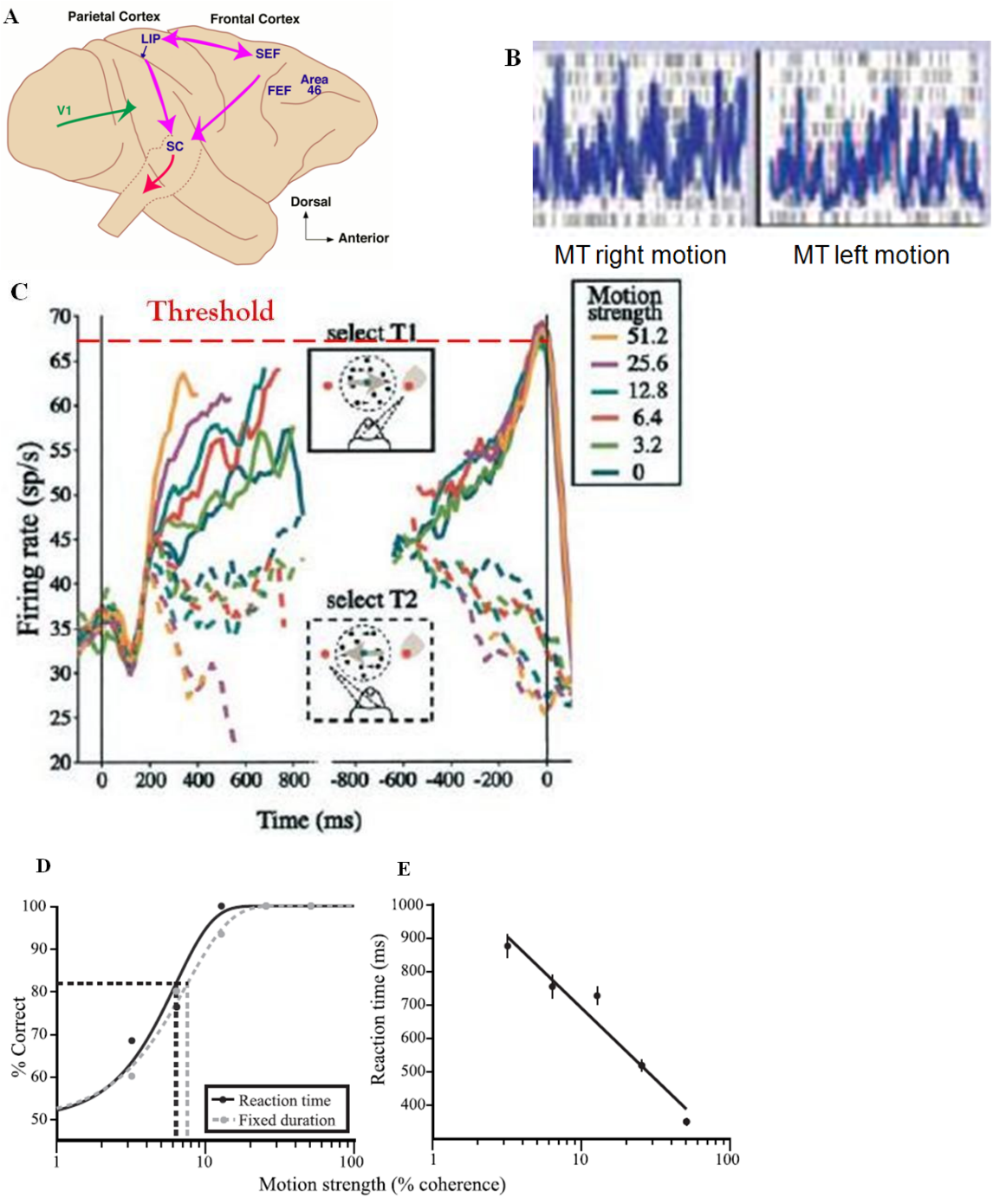

Figure 2: A) Electrophysiological recordings in primates identify neural systems involved in perceptual decision-making. B) Firing-Rates of neurons in the area MT, selective for leftward direction of motion and rightward motion [15]. C) Firing-rates of neurons in the area LIP selective for leftward saccades, for different motion strengths. Solid lines represent saccadic choices toward the leftward target (T1), dotted lines represent saccades made toward the rightward target (T2). The firing-rates of neurons selective for rightward saccades when the motion is towards the left are assumed to have time-courses similar to that for a leftward selective neuron when a rightward saccade is made. The time at which the firing-rates cross a threshold is correlated with the behavioral Reaction Time. D) Psychometric function relating Accuracy to % coherence. E) Reaction Times as a function of motion-strength. Reproduced from [22].

ing of motion) that were selective towards leftward motion (Fig. 5 B). However, the firing rates of the neurons in the MT were not time-dependent, depending linearly on the motion coherence. The firing-rates of both the selective and non-selective populations remained noisy, and determining the decision from this pattern would be inaccurate, being merely reflective of the inherent uncertainty present in the stimulus and its consequent neural representation. Firing-rate patterns observed in the LIP (involved in the processing of eye-movements) displayed a ramping up of activity over time for the neural populations selective for the corresponding direction of motion, correlated with the decision rendered, together with a decay of firing rate activity for the populations selective towards the opposite direction (Fig. 5 C). Critically, the time at which these firing-rates cross a fixed threshold just before the saccadic decision is made, yields the RTs for behavioral performance. The ramping up to this decision threshold was faster for larger motion-strengths [5, 22, 29]. Behavioral findings such as psychometric functions relating accuracy to coherence revealed greater accuracy when the coherence was higher (Fig. 5 D). Similarly, RTs were shorter for higher coherences, reflecting faster ramping up to the decision threshold (Fig. 5 E) [22]. Taken together, these results suggest that in such perceptual choice experiments, noisy signals regarding the stimulus are relayed from the MT to the LIP, where the evidence favoring the two alternatives is integrated over time [30].

6 The Decision Problem

In order to mathematically model this decision process, we consider 2 neuronal populations whose firing rates (activities) provide evidence for 2 alternatives. Let the population-averaged mean neural activities of the competing populations be $I_1(t) = I_1$ and $I_2(t) = I_2$, respectively. I then reflects the amount of evidence accumulated favoring each choice at any particular time. Each population has independent random fluctuations with the same standard deviation $\sigma(t) = \sigma$. The evidence in favor of each alternative is integrated over time. The goal of the decision process is to determine which of I_1 and I_2 is greater at the moment the decision is made. The presence of noise introduces a speed-accuracy tradeoff. A fixed low threshold for the accumulation process causes the decision to be fast but inaccurate whereas a higher fixed threshold allows more time for the noise to be averaged out, but accumulation takes place over a longer time. The optimum decision problem can be defined as: given I_1, I_2, σ: what strategy yields
a) The highest accuracy (lowest Error Rate: $ER = P(Error)$, the probability of making errors), given a fixed Decision Time (DT), corresponding to what is known as the Interrogation Paradigm, or
b) The shortest Response Time ($RT = DT + T_0$, where T_0 is the time due to sensory-motor processes) given the Error Rate (ER). This is an example of the Free-Response Paradigm wherein subjects implicitly choose a tradeoff to maximize their reward.

Consider Y, a random variable that computes the difference in activity of the 2 populations. Successive samples of Y in each trial are drawn from 1 of 2 probability distributions $p_1(y)$ and $p_2(y)$ with means m_1 and m_2. We wish to find which of

hypotheses $H_1(I_1 - I_2 = m_1 > 0)$ or $H_2(I_1 - I_2 = m_2 < 0)$ is correct. For the Interrogation Paradigm (minimize ER subject to fixed DT) the *Neyman-Pearson* [16] procedure is used. In order to find from which distribution a random sequence $Y = y_1, y_2, , y_n$ is drawn, we calculate the *likelihood ratio* of Y, given H_1, H_2

$$\frac{p_{1_n}}{p_{2_n}} = \frac{p_1(y_1)p_1(y_2)...p_1(y_n)}{p_2(y_1)p_2(y_2)...p_2(y_n)} \tag{6.1}$$

We consider all observations to be independent. Then p_{1_n} and p_{2_n} give the probability of observing the *sequence of observations* under H_1 and H_2, respectively. H_1 is accepted if the ratio in Eq.(6.1) is greater than Z where Z is a constant determining the level of accuracy for H_1 or H_2. For a fixed n (corresponding to a fixed DT) and $Z = 1$, this procedure yields the minimum error probability $P(Error)_{min}$, making it optimal for the Interrogation Paradigm. For the Free-Response Paradigm (Minimize DT, subject to fixed ER) the *Sequential Probability Ratio Test* (SPRT) is used [1, 34]. In this case, observations continue as long as

$$Z_2 < \frac{p_{1_n}}{p_{2_n}} < Z_1 \tag{6.2}$$

We assume $Z_2 < Z_1$. If $\frac{p_{1_n}}{p_{2_n}} > Z_1$ then $H_1(I_1 - I_2 = m_1 > 0)$ is accepted but if $\frac{p_{1_n}}{p_{2_n}} < Z_2$ then $H_2(I_1 - I_2 = m_2 < 0)$ is accepted. Among all fixed or variable sample decision methods that give fixed error probability, SPRT minimizes the number of samples n [35] (corresponding to Minimum DT). Thus the SPRT is optimal for the Free-Response Paradigm. Now if we take logarithms in Eq.(6.1) and Eq.(6.2), then accumulation continues as long as

$$\log Z_2 < \sum_{i=1}^{n} \log \frac{p_1(y_i)}{p_2(y_i)} < \log Z_1 \tag{6.3}$$

That is the accumulation process is given by

$$I^n = I^{n-1} + \log \frac{p_1(y_n)}{p_2(y_n)} \tag{6.4}$$

Then Eq. (6.4) is a random walk starting at I_0 and accumulation continues till $I_n > \log Z_1$ or $I_n < \log Z_2$.

7 Drift Diffusion Model (DDM)

We observe that as discrete samples are taken more frequently, the discrete log-likelihood ratio I_n in Eq. (6.4) becomes the continuous random variable $x(t)$. We integrate the difference between evidence for 2 alternatives H_1 and H_2 where $x(t)$ is the accumulated value of the difference at time t. Then the pure *Drift Diffusion Model* (DDM) is given by the first order stochastic differential equation (SDE):

$$dx = A\ dt + \sigma\ dW, \qquad x(0) = 0 \tag{7.1}$$

where $A\ dt$ represents the average increase in evidence supporting the correct choice per unit time. Note that $A > 0$ if H_1 is correct and $A < 0$ if H_2 is correct. $\sigma\ dW$ is white noise, Gaussian distributed with Mean 0 and Variance $\sigma^2\ dt$.

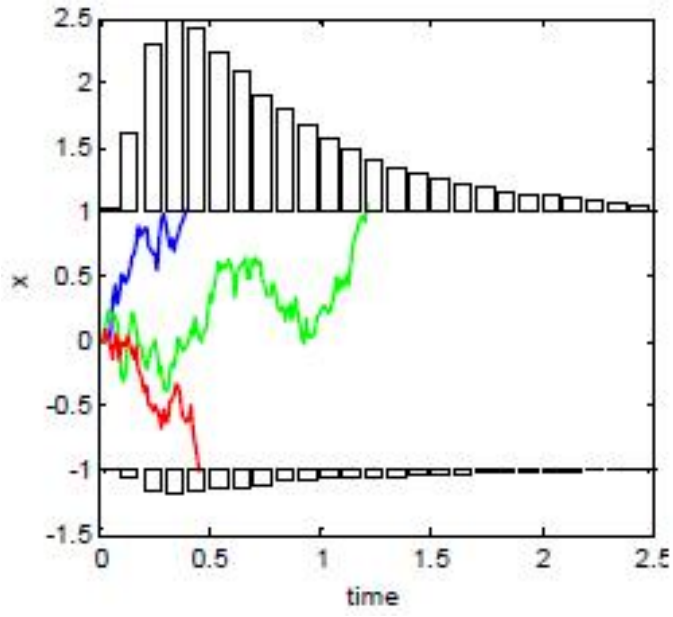

Figure 3: Time evolution of the Drift Diffusion Model (DDM) showing accumulated difference between the evidence for the two alternatives as a function of time. The model was simulated for 100,000 trials using the Euler method with timestep $dt = 0.01$, drift rate $A = 0.1$, $\sigma = 1$ and threshold $z = 1$. Several sample paths are shown. The histograms show the number of paths reaching the corresponding thresholds after a particular time interval.

Thus, on average, x grows at the drift rate A but solutions diffuse owing to the presence of noise. Sample paths may therefore cross the the incorrect threshold, yielding errors (Fig. 3). Note that

$$x(t) \propto I_n \tag{7.2}$$

where $t = n\Delta t$, and Δt is the time between samples I_{n-1} and I_n. Hence the DDM implements the Neyman-Pearson procedure for $Z = 1$ for the Interrogation Paradigm and the SPRT for the Free-Response Paradigm, making it the *optimal* decision maker.

The DDM is useful, however, for modeling simple decision tasks [20]. Complex decision tasks, which involve the accumulation of reward biases, stimulus histories and attentional shifts require additional features such as time-varying drift-rates [11], or other models such as the Ornstein-Uhlenbeck (O-U) model or the Leaky Competing Accumulator (LCA) model [32].

8 Leaky Competing Accumulator Model (LCA)

The Leaky Competing Accumulator (LCA) Model, alternatively known as the Mutual Inhibition Model of Decision Making in Two-Alternative Forced-Choice (TAFC) tasks (Fig.4) is described by the ordinary stochastic differential equations (SDEs):

$$\begin{aligned} dx_1 &= [\rho_1 - kx_1 + \alpha f(x_1) - \beta f(x_2)]\,\frac{dt}{\tau} + \sigma dW_1 \\ dx_2 &= [\rho_2 - kx_2 + \alpha f(x_2) - \beta f(x_1)]\,\frac{dt}{\tau} + \sigma dW_2 \end{aligned} \tag{8.1}$$

where x_1 and x_2 represent the two decision variables corresponding to the input currents received by the populations selective for the two alternatives and f represents the firing-rates of these populations. This input current-output firing-rate function f can vary in its degreee of non-linearity. It can be linear, piecewise linear, threshold-linear or the non-linear logistic function. ρ_1 and ρ_2 represent the input signals relayed from the MT. These depend on the motion-coherence. α, k and β represent the recurrent self-excitation, leak and mutual inhibition, respectively. τ represents a time-constant that determines how fast or how slow the evidence accumulation takes place. Note that $\tau > 0$. dW_1 and dW_2 are independent Wiener process increments drawn from a normal distribution. That is, $dW_j = \sqrt{\frac{dt}{\tau}}N(0,1)$. We consider these noise processes to have a standard deviation σ. We assume the initial conditions $x_1(0) = x_2(0) = 0$.

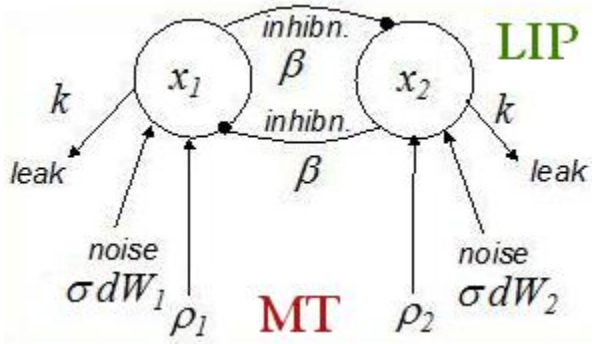

Figure 4: The Leaky Competing Accumulator Model of perceptual decision-making. The two decision units x_1 and x_2 represent neural populations in the LIP selective for leftward and rightward saccades. These leaky, mutually-inhibitory populations receive noisy input signals from the MT.

In order to explore meaning of each parameter in greater detail, consider the noise-free ordinary differential equations ($dW_j = 0$). In the absence of inhibition ($\beta = 0$), and signals from the MT ($\rho_1 = \rho_2 = 0$), Eq. (8.1) reduces to $\frac{dx_i}{dt} = -\frac{k}{\tau}x_i$. Since the leak k is always positive, the activity of each of the decision variables decay to baseline ($x(t) = e^{-t/\tau}$). The mutual inhibition β expresses the amount by which two neural populations inhibit one another's activities. This is evident if we consider

$\rho_1 = \rho_2 = 0, k = 0$ in the deterministic version of Eq.(8.1). The greater the input-current x_1, the greater its firing-rate $f(x_1)$, the greater is the inhibition of the decision variable x_2 and vice-versa. This ensures that when x_1 and hence $f(x_1)$ is ramping up, x_2 and consequently $f(x_2)$ is ramping down, enabling a categorical decision to be rendered, in a manner similar to that observed in electrophysiological experiments. α represents recurrent self-excitation. If we set all other parameters except α to zero, then Eq. (8.1) becomes $\frac{dx_i}{dt} = \frac{\alpha}{\tau} f(x_i)$. Since $\alpha \geq 0$, the input-currents x_i and the firing-rates $f(x_i)$ keep increasing, which corresponds to the populations being self-excited.

In subsequent subsections, we analyze the dynamics of the model in each case in f. For simplicity we shall assume $\alpha = 0$, as in [8], though this restriction shall be removed while studying more complex variations of the LCA. We place particular emphasis on studying the phase plane of the models in different parameter regimes. Particularly, we consider whether fixed points exist, and if so whether they are unstable or stable. Determining whether asymetrical, stable fixed points $x_1^* \neq x_2^*$ exist for the decision making system, and if so, where they are located, or equivalently, which of x_1^* or x_2^* is greater, is imperative for determining the decision rendered.

If the fixed point is a saddle, then it represents a point where $x_1(t)$ and $x_2(t)$ become unequal and diverge such that one increases while the other is inhibited towards baseline. This corresponds to the point of splitting between firing-rates (obtained by computing $f(x_i(t))$) of the two populations selective towards the leftward or rightward saccade generating stimuli Fig. (5 C) observed in primate electrophysilogy experiments [22].

In our analysis, we consider 3 cases, when the network is leak dependent: $\beta < k$, balanced: $\beta = k$ or inhibition dependent $\beta > k$. In predominantly leaky networks, information that is accumulated during the earlier parts of a trial is lost and greater importance is placed on information relayed to the decision network during the later parts. The inverse is true for inhibition dependent networks. We thus demonstrate that the relative magnitudes of leak and inhibition play a major role in the dynamics of the decision process.

We also deduce that not only does the degree of coherence C of the dot motion stimulus determine how fast neural firing rates increase or decrease, but also determines where in the phase plane the fixed points lie. We derive coherence ranges for the the location and nature of the fixed points in closed form. Whereas previous work has studied the effect of different gains of neural input-output functions [8] as discussed below, we explore the effects of the degree of non-linearity and different coherences in LCA models of perceptual decision-making.

We assume $k, \beta > 0$ and $\rho_1 + \rho_2 = 1, \rho_1, \rho_2 \in [0, 1]$. Let $\rho_1 - \rho_2 = C \in [-1, 1]$. Thus,

$$\begin{aligned} \rho_1 &= 0.5(1 + C) \\ \rho_2 &= 0.5(1 - C) \end{aligned} \tag{8.2}$$

Then Eq. (8.1) becomes

$$
\begin{aligned}
dx_1 &= [\rho_1 - kx_1 - \beta f(x_2)]\,\frac{dt}{\tau} + \sigma dW_1 \\
dx_2 &= [\rho_2 - kx_2 - \beta f(x_1)]\,\frac{dt}{\tau} + \sigma dW_2
\end{aligned} \tag{8.3}
$$

If $f(x) = x$, we can orthogonally transform the linear system into uncoupled coordinates (Fig. 5).

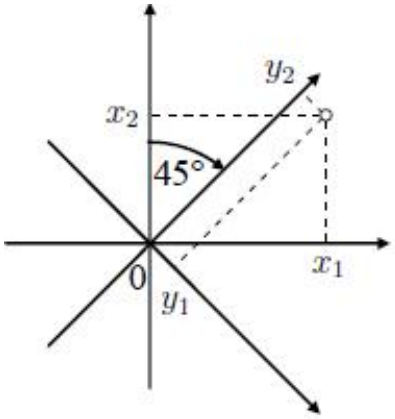

Figure 5: Orthogonal tranformation into two decoupled processes.

$$
y_1 = \frac{x_1 - x_2}{\sqrt{2}} \tag{8.4}
$$

$$
y_2 = \frac{x_1 + x_2}{\sqrt{2}} \tag{8.5}
$$

Note that, since the Wiener noise processes are assumed to be independent,

$$
\frac{1}{\sqrt{2}}\acute{\sigma}d\acute{W}_j = \frac{1}{\sqrt{2}}(\sigma dW_1 \pm \sigma dW_2) = \frac{1}{\sqrt{2}}\sqrt{\sigma^2+\sigma^2}d\acute{W}_j = \frac{\sqrt{2}}{\sqrt{2}}\sigma d\acute{W}_j = \sigma d\acute{W}_j \tag{8.6}
$$

Then the 2-dimensional LCA model given by Eq.(8.3) reduces to two uncoupled 1-dimensional Ohrnstein-Uhlenbeck (OU) processes

$$
dy_1 = \left[\frac{\rho_1 - \rho_2}{\sqrt{2}} + (\beta - k)y_1\right]\frac{dt}{\tau} + \sigma dW_1' \tag{8.7}
$$

$$
dy_2 = \left[\frac{\rho_1 + \rho_2}{\sqrt{2}} - (\beta + k)y_2\right]\frac{dt}{\tau} + \sigma dW_2' \tag{8.8}
$$

Neglecting the noise dW_2', Eq. (8.8) has a fixed point at when $\frac{dy_2}{dt} = 0$. Then $y_2^* = \frac{\rho_1+\rho_2}{\sqrt{2}(\beta+k)} = \frac{1}{\sqrt{2}(\beta+k)}$. Let $\frac{dy_2}{dt} = F_2(y_2) = \left[\frac{\rho_1+\rho_2}{\sqrt{2}} - (\beta+k)y_2\right]\frac{1}{\tau}$. In order to determine the stability of this fixed point, we perform a linear stability analysis as described in Section 2.

Perturbations from the fixed point grow exponentially if $F_2^{'}(y_2^*) > 1$, making the fixed point unstable and decay if $F_2^{'}(y_2^*) < 1$, enabling a stable fixed point. Note that for this OU model obtained from reducing the LCA model,

$$F_2^{'}(y_2^*) = -\frac{\beta + k}{\tau} < 0 \tag{8.9}$$

This fixed point is stable since $\beta, k > 0$ and $\rho_1, \rho_2 \geq 0$.
Now, let $\frac{dy_1}{dt} = F_1(y_1) = \left[\frac{\rho_1 - \rho_2}{\sqrt{2}} + (\beta - k)y_2\right]\frac{1}{\tau}$ Note that, Eq. (8.7) has a fixed point at $y_1^* = \frac{\rho_1 - \rho_2}{\sqrt{2}(\beta - k)} = \frac{C}{\sqrt{2}(\beta - k)}$. Performing a similar linear stability analysis, we note that

$$F_1^{'}(y_1^*) = \frac{\beta - k}{\tau}. \tag{8.10}$$

The stability of this fixed point, however, depends on the sign of $\beta - k$. Thus Eq.(8.8) is a stable OU process whereas Eq. (8.7) is stable if $\beta - k < 0$ and unstable if $\beta - k > 0$. Since in the interrogation protocol the decision made depends on whether x_1 or x_2 is greater at the interrogation time T, (that is, Alternative 1 is chosen if $x_1(T) > x_2(T)$ and vice versa), the decision depends on the sign of $y_1(T)$. If $y_1(T) > 0$ then Alternative 1 is chosen and if $y_1(T) < 0$ then Alternative 2 is chosen. We need only consider the OU process given by Eq. (8.8)

$$dy_1 = [\lambda y_1 + A]\frac{dt}{\tau} + \sigma dW \tag{8.11}$$

where $A = \frac{\rho_1 - \rho_2}{\sqrt{2}}$ and $\lambda = \beta - k$. When $\lambda = 0$ the OU process simplifies to the Drift Diffusion Model (DDM)

$$dy_1 = A\frac{dt}{\tau} + \sigma dW \tag{8.12}$$

The evolution of the probability distribution function for Eq. (8.11) $p(y_1, t)$ is governed by the forward Fokker-Planck or Kolmogorov Equation

$$\frac{\partial p}{\partial t} = -\frac{\partial}{\partial x}\left[(A(t) + \lambda y_1)p\right] + \frac{\sigma^2}{2}\frac{\partial^2 p}{\partial x^2} \tag{8.13}$$

We assume that $p(y_1, 0) = \delta(y_1 - \mu_0)$, where μ_0 is the mean of the probability distribution function at time $t = 0$ and δ is the Dirac-delta function. Solutions to Eq. (8.13) is given by

$$p(y_1, t) = \frac{1}{\sqrt{2\pi\nu(t)}}\exp\left[-\frac{(y_1 - \mu(t))^2}{2\nu(t)}\right] \tag{8.14}$$

$$\mu(t) = \mu_0 e^{\lambda t} + \int_0^t e^{\lambda(t-s)}A(s)ds \tag{8.15}$$

$$\nu(t) = \frac{\sigma^2}{2\lambda}(e^{2\lambda t} - 1) \tag{8.16}$$

If $\lambda = 0$ then Eq. (8.15) and Eq. (8.16) respectively reduce to

$$\mu(t) = \mu_0 + \int_0^t A(s)ds \tag{8.17}$$

$$\nu(t) = \sigma^2 t \tag{8.18}$$

The probability of choosing Alternative 1 is given by

$$\begin{aligned} P_{choose1}(T) &= \int_0^\infty p(y_1, t)dy_1 \\ &= \frac{1}{2}\left[1 + erf\left(\frac{\mu(T)}{\sqrt{2\nu(T)}}\right)\right] \end{aligned} \tag{8.19}$$

In the analyses that shall follow, we shall let $k = 1$ and allow β to assume the values 0.5,1 and 1.5. Therefore λ can be either -0.5 (stable OU), 0 (DDM) or +0.5 (unstable OU). Other parameters include $dt = 1$, $\tau = 10$ (hence $dt/\tau = 0.1$)and $\sigma = \frac{0.2214}{\sqrt{(2)}} = 0.158, T = 100$ iterations.

8.1 Input Current-Output Firing Rate Functions

We let f in Eq. (8.3) be different functions and that vary in their degree of non-linearity and observe whether the dynamics of the model vary significantly or remain similar. Specifically, as in [8] we consider f to be the non-linear logistic equation

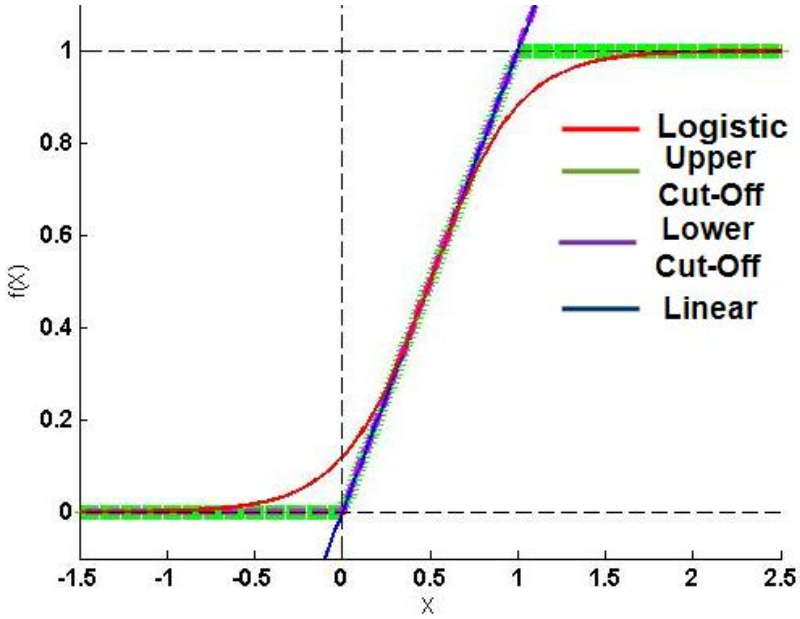

Figure 6: Input Current-Ouput Firing-Rate functions f varying in their degree of nonlinearity. All of them have slope or gain $g = 1$ and shift $b = 0.5$

$$f(x) = \frac{1}{1 + exp\,(-4g(x-b))} \tag{8.20}$$

where g and b determine the maximal slope and shift.$f(b) = \frac{1}{2}$ and $f^{'}(b) = g$ (Fig.6).Let $g = 1$ and $b = 0.5$. Then Eq. (8.20) is bounded between 0 and 1. Eq. (8.20) can be approximated as the threshold-linear function

$$f(x) = \begin{cases} 0 & \text{if } x \in (-\infty, b - \frac{1}{2g}) \\ x & \text{if } x \in [b - \frac{1}{2g}, b + \frac{1}{2g}] \\ 1 & \text{if } x \in (b + \frac{1}{2g}, \infty) \end{cases} \tag{8.21}$$

Eq. (8.21) is linear except for a lower cut-off at 0 and an upper cut-off at 1. Eq. (8.21) can be further approximated as

$$f(x) = \begin{cases} 0 & \text{if } x \in (-\infty, b - \frac{1}{2g}) \\ x & \text{if } x \in [b - \frac{1}{2g}, \infty) \end{cases} \tag{8.22}$$

which is linear except for a lower cut-off at 0. In similar vein, as in [32] we can let f be the identity function under the assumption that activations less than zero are truncated to zero. In this case, the firing-rates are considered to be equal to the input currents, and since firing-rates of neurons cannot be negative, they are dynamically set to zero, if they become negative. Equivalently, $x_i(t) = \max(x_i(t), 0)$ in Eq. (8.3). We denote this the truncated activation case. Finally, we can completely linearize Eq. (8.20), assuming f to be the identity function.

8.2 Deterministic System

Considering the Leaky Competing Accumulator to be a noise-free system, Eq. (8.3) becomes a system of completely determinisitc ordinary differential equations (ODEs). We can compute the fixed points of this noise-free system using its nullclines.

$$x_1 = \frac{\rho_1 - \beta f(x_2)}{k} \tag{8.23}$$

$$x_2 = \frac{\rho_2 - \beta f(x_1)}{k} \tag{8.24}$$

Note that $\frac{dx_1}{dt} = 0$ on Eq. (8.23) and $\frac{dx_2}{dt} = 0$ on Eq. (8.24).

8.3 Stability Analysis of Network Models

In order to determine the stability of the fixed points, we assume $\frac{dx_1}{dt} = F(x_1, x_2)$ and $\frac{dx_2}{dt} = G(x_1, x_2)$ and perform a linear stability analysis as described in Section 2.

For the Leaky Competing Accumulator model, in particular the Jacobian matrix becomes

$$J(x_1^*, x_2^*) = \begin{pmatrix} -k & -\beta f^{'}(x_2^*) \\ -\beta f^{'}(x_1^*) & -k \end{pmatrix} \tag{8.25}$$

The trace of this matrix is $\tau = trace(J) = -2k$ and the determinant $\Delta = \det(J) = k^2 - \beta^2 f^{'}(x_1^*) f^{'}(x_2^*)$.

There exist different cases depending on the values of k, β, ρ_1 and ρ_2. We shall analyze the phase-plane in each of the cases $k > \beta$: the leak dependent LCA (corresponding to stable OU process when f is linear), $k < \beta$:the inhibition dependent LCA (corresponding to an unstable OU process) and $k = \beta$: the balanced LCA(corresponding to the DDM).

8.3.1 Linear

Performing the linear stability analysis, we note that $f^{'}(x_1^*) = 1 = f^{'}(x_2^*)$ and thus

$$J(x_1^*, x_2^*) = \begin{pmatrix} -k & -\beta \\ -\beta & -k \end{pmatrix} \tag{8.26}$$

Note that the trace $\tau = -2k$ and the determinant $\Delta = k^2 - \beta^2$. In order to find the eigenvalues Λ of the Jacobian matrix, we solve the characteristic polynomial equation

$$\begin{aligned} \Lambda^2 - \tau\Lambda + \Delta &= 0 \\ \Rightarrow \Lambda^2 + 2k\Lambda + k^2 - \beta^2 &= 0 \end{aligned} \tag{8.27}$$

This yields two eigenvalues $\Lambda_1 = \beta - k$ and $\Lambda_2 = -(\beta + k) < 0$. Note that when $\lambda = \beta - k < 0$, then $\Lambda_1 < 0$,and the fixed point is a sink, whereas when $\lambda > 0$ then $\Lambda_1 > 0$, and the fixed point is a saddle. Note that $|\Lambda_2| > |\Lambda_1|$ since $\beta + k > \beta - k$. Hence, when the fixed point is a saddle, trajectories rapidly move to the decision line

$$y_2 = \frac{x_1 + x_2}{\sqrt{2}} = \frac{\rho_1 + \rho_2}{\sqrt{2}(\beta + k)} \tag{8.28}$$

and progress along it.

8.3.2 Piecewise linear: Lower Cut-Off

For the LCA system given by Eq. (8.3) with the Lower Cut-Off function Eq. (8.22), for fixed points in Quadrant I ($x_1^*, x_2^* > 0$), the stability is identical to the linear case. Otherwise, for fixed points in Quadrants II or IV, $f(x_1^*) = 0$ or $f(x_2^*) = 0$. It follows that $f^{'}(x_1^*) = 0$ or $f^{'}(x_2^*) = 0$

Thus, referring to Eq. (8.25), $\tau = -2k$ and $\Delta = k^2$. Solving the charactersistic polynomial, we obtain the eigenvalues $\Lambda_1 = \Lambda_2 = -k < 0$. Thus in this case, the fixed point is a sink.

8.3.3 Threshold linear: Upper and Lower Cut-Off

For the Upper Cut-Off function given in Eq. (8.21), the analysis is similar to that for the lower cut-off function. Note that when $x_1^* \geq 1$ or $x_2^* \geq 1$ then $f(x_1^*) = 1$ or $f(x_2^*) = 1$, respectively. It follows that $f^{'}(x_1^*) = 0$ or $f^{'}(x_2^*) = 0$ and the fixed points are sinks.

8.4 Leak Dependent LCA: $\beta < k$, $\lambda < 0$

Figure 7 shows the phase-plane with the nullclines, the decision line and a sample trajectory for $C \in \left(\frac{\beta-k}{\beta+k} - \frac{\beta-k}{\beta+k}\right)$. Another case (not shown here) occurs when $C \in \left[-\frac{\beta-k}{\beta+k}, 1\right]$, respectively. When $C \in \left[-1, \frac{\beta-k}{\beta+k}\right]$, the case is symmetric. Note that the trajectories approach the decision line and move along it to a stable fixed point. We discuss the various fixed points of the different types of LCA models, which differ from eachother in the choice of the function f, beginning with the linear identity function and then considering progressively non-linear versions of f.

8.4.1 Linear

When $f(x) = x$, we can solve the nullclines Eq. (8.23) and Eq. (8.24) to obtain

$$\begin{aligned} kx_1 + \beta x_2 &= \rho_1 \\ kx_2 + \beta x_1 &= \rho_2 \end{aligned} \tag{8.29}$$

or equivalently,

$$\begin{pmatrix} x_1 \\ x_2 \end{pmatrix} = \frac{1}{k^2 - \beta^2} \begin{pmatrix} k & -\beta \\ -\beta & k \end{pmatrix} \begin{pmatrix} \rho_1 \\ \rho_2 \end{pmatrix}$$

We obtain the unique fixed point $(x_1, x_2)^* = \left(\frac{\rho_1 k - \rho_2 \beta}{k^2-\beta^2}, \frac{\rho_2 k - \rho_1 \beta}{k^2-\beta^2}\right)$. Note that this fixed point is always stable. The unique fixed point can be in one of 3 quadrants, depending on the value of C and hence ρ_1 and ρ_2. We observe that $x_1^*, x_2^* > 0$ when

$$\begin{aligned} \frac{\rho_1 k - \rho_2 \beta}{k^2 - \beta^2} &> 0 \\ \frac{0.5(1+C)k - 0.5(1-C)\beta}{k^2 - \beta^2} &> 0 \\ C(k+\beta) &> \beta - k \\ C &> \frac{\beta - k}{\beta + k} \end{aligned} \tag{8.31}$$

and similarly,

$$\begin{aligned} \frac{\rho_2 k - \rho_1 \beta}{k^2 - \beta^2} &> 0 \\ \frac{0.5(1-C)k - 0.5(1+C)\beta}{k^2 - \beta^2} &> 0 \\ C(k+\beta) &< -(\beta - k) \\ C &< -\frac{\beta - k}{\beta + k} \end{aligned} \tag{8.32}$$

that is, when $C \in \left(\frac{\beta-k}{\beta+k}, -\frac{\beta-k}{\beta+k}\right)$ (Fig.7).
If $x_1^* \leq 0, x_2^* > 0$ then

$$\begin{aligned} \frac{\rho_1 k - \rho_2 \beta}{k^2 - \beta^2} &\leq 0 \\ \frac{0.5(1+C)k - 0.5(1-C)\beta}{k^2 - \beta^2} &\leq 0 \\ C(k+\beta) &\leq \beta - k \\ -1 \leq C &\leq \frac{\beta - k}{\beta + k} \end{aligned} \tag{8.33}$$

that is, when $C \in \left[-1, \frac{\beta-k}{\beta+k}\right]$. Finally, $x_1^* > 0, x_2^* \leq 0$ when

$$\begin{aligned} \frac{\rho_2 k - \rho_1 \beta}{k^2 - \beta^2} &\leq 0 \\ \frac{0.5(1-C)k - 0.5(1+C)\beta}{k^2 - \beta^2} &\leq 0 \\ C(k+\beta) &\geq -(\beta - k) \\ -\frac{\beta - k}{\beta + k} \leq C &\leq 1 \end{aligned} \tag{8.34}$$

that is, $C \in \left[-\frac{\beta-k}{\beta+k}, 1\right]$.

For our chosen parameter values of $k = 1, \beta = 0.5$, $\frac{\beta-k}{\beta+k} = -\frac{1}{3}$.

8.4.2 Truncated Activation

The nullclines for Eq. (8.3) with the criterion $x_i(t) = \max(x_i(t), 0)$ are shown in Fig.7, upper right panel. When $k > \beta$, the system has a set of fixed points. The fixed points are stable and always in the first (non-negative) quadrant. The fixed point is $(x_1, x_2)^* = \left(\frac{\rho_1 k - \rho_2 \beta}{k^2 - \beta^2}, \frac{\rho_2 k - \rho_1 \beta}{k^2 - \beta^2}\right)$ for the same values of C as in the linear case. Solving using the nullclines

$$x_1 = max\left(\frac{\rho_1 - \beta x_2}{k}, 0\right) \tag{8.35}$$

$$x_2 = max\left(\frac{\rho_2 - \beta x_1}{k}, 0\right) \tag{8.36}$$

In addition, we have a set of fixed points as a consequence of dynamically clamping either $x_1(t)$ or $x_2(t)$ to zero. We note that when $x_1^* = 0$, $x_2^* = \frac{\rho_2}{k}$ and when $x_2^* = 0$, $x_1^* = \frac{\rho_1}{k}$. The fixed point is thus $(x_1, x_2)^* = \left(0, \frac{\rho_2}{k}\right)$ for $C \in \left[-1, \frac{\beta-k}{\beta+k}\right)$ and $(x_1, x_2)^* = \left(\frac{\rho_1}{k}, 0\right)$ for $C \in \left(-\frac{\beta-k}{\beta+k}, 1\right]$.

8.4.3 Piecewise linear: Lower Cut-Off

When we use the piece-wise linear function Eq. (8.22), we once again obtain a unique and stable fixed point for the $k > \beta$ case. The fixed point is the same as in the linear and truncated activation cases when $C \in \left(\frac{\beta-k}{\beta+k}, -\frac{\beta-k}{\beta+k}\right)$ (Fig. 7, middle panel, left). When $C \in \left[-1, \frac{\beta-k}{\beta+k}\right]$, then $x_1 \leq 0, x_2 > 0$ and hence $f(x_1) = 0$ and $f(x_2) = x_2$. Thus solving the nullclines,

$$\begin{aligned} kx_1 + \beta x_2 &= \rho_1 \\ kx_2 &= \rho_2 \end{aligned} \tag{8.37}$$

we obtain the fixed point $(x_1, x_2)^* = \left(\frac{\rho_1 k - \rho_2 \beta}{k^2}, \frac{\rho_2}{k}\right)$.

Similarly when $C \in \left[-\frac{\beta-k}{\beta+k}, 1\right]$, then $x_1 > 0, x_2 \leq 0$ and thus $f(x_2) = 0$ and $f(x_1) = x_1$, we solve the nullclines,

$$\begin{aligned} kx_1 &= \rho_1 \\ kx_2 + \beta x_1 &= \rho_2 \end{aligned} \tag{8.38}$$

We obtain the corresponding fixed point $(x_1, x_2)^* = \left(\frac{\rho_1}{k}, \frac{\rho_2 k - \rho_1 \beta}{k^2}\right)$.

8.4.4 Threshold Linear: Upper and Lower Cut-Offs

The derivations for the Lower Cut-Off case can be repeated in order to determine the stable unique fixed point for the case when f is the threshold linear function Eq. (8.21), as long as $x_1, x_2 \leq 1$. That is, f is the identity function except for a lower cut-off at 0 and an upper cut-off at 1. The same fixed points are obained for the corresponding values of C (Figs. 7,middle panel, right). However, ignoring the conditions $\rho_1 + \rho_2 = 1, \rho_1, \rho_2 \in [0, 1]$,we can derive additional possible values that the fixed point can assume. Specifically, if $x_1, x_2 > 1$, then $f(x_1) = f(x_2) = 1$ and the nullclines of Eq. (8.3) yield

$$\begin{aligned} kx_1 + \beta &= \rho_1 \\ kx_2 + \beta &= \rho_2 \end{aligned} \tag{8.39}$$

Solving this system gives us the fixed point $(x_1, x_2)^* = \left(\frac{\rho_1 - \beta}{k}, \frac{\rho_2 - \beta}{k}\right)$. The fixed point cannot attain this value under the above constraints and parameter choices, since it requires $\rho_1, \rho_2 > \beta + k$ or equivalently,
$\rho_1 + \rho_2 > 2(\beta + k) > 1$. When $x_1 > 1$ and $x_2 < 0$ then $f(x_1) = 1$ and $f(x_2) = 0$. Then the nullclines reduce to

$$\begin{aligned} kx_1 &= \rho_1 \\ kx_2 + \beta &= \rho_2 \end{aligned} \tag{8.40}$$

This yields the fixed point $(x_1, x_2)^* = \left(\frac{\rho_1}{k}, \frac{\rho_2-\beta}{k}\right)$. Similarly, the symmetric condition of $x_1 < 0, x_2 > 1$ yields the fixed point $(x_1, x_2)^* = \left(\frac{\rho_1-\beta}{k}, \frac{\rho_2}{k}\right)$. This value of the fixed point is also not possible under the current constraints and parameterization. Finally, when $x_1 > 1$ and $0 < x_2 < 1$, then $f(x_1) = 1$ and $f(x_2) = x_2$ and the nullclines give

$$\begin{aligned} kx_1 + \beta x_2 &= \rho_1 \\ kx_2 + \beta &= \rho_2 \end{aligned} \tag{8.41}$$

which yield the fixed point $(x_1, x_2)^* = \left(\frac{\rho_1 k-\rho_2\beta+\beta^2}{k^2}, \frac{\rho_2-\beta}{k}\right)$. The symmetric condition $0 < x_1 < 1, x_2 > 1$ yields the fixed point $(x_1, x_2)^* = \left(\frac{\rho_1-\beta}{k}, \frac{\rho_2 k-\rho_1\beta+\beta^2}{k^2}\right)$. As in the case above, the fixed point cannot attain this value under the current parameterization and constraints. Later, we may alter the constraints to enable the fixed points to attain these values.

8.4.5 Logistic

The non-linear LCA model Eq. (8.3) with f as the logistic function Eq. (8.20) and gain $g = 1$ always has a stable, unique fixed point irrespective of the relative values of k and β(Fig. 7, bottom panel). It is not true that for corresponding values of C, the fixed point lies in the same quadrant as the stable, unique fixed point for the lower cut-off and upper and lower cut-off cases. Henceforth we do not separately include the logistic case in our discussion of the phase-plane dynamics of the different LCA models when $\lambda = 0$ or $\lambda > 0$.

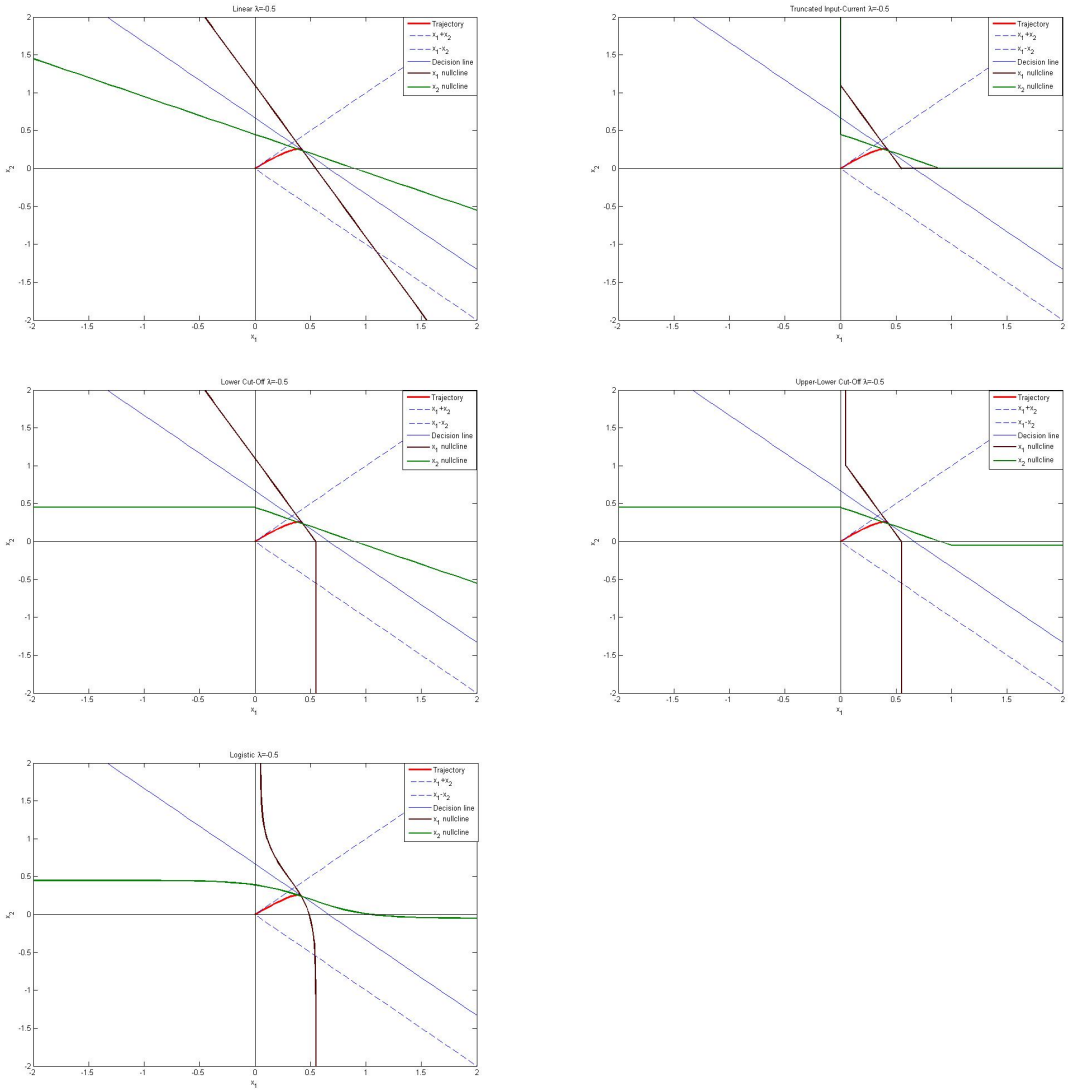

Figure 7: Phase-Plane for the Leak Dependent LCA, i.e.,when $\lambda = \beta - k < 0$ and Coherence $C \in \left(\frac{\beta-k}{\beta+k} - \frac{\beta-k}{\beta+k}\right)$.Y-axis represents the activity of the decision variable or input-current x_2 and the x-axis represents the activity of the decision variable x_1. The decision line given by Eq. (8.28) is represented by a solid blue line. Brown and green curves correspond to the nullclines for x_1 and x_2 respectively. A point of intersection of the nullclines yields a fixed point. Dashed lines represent the orthogonally transformed coordinates $y_1 = x_1 - x_2$ and $y_2 = x_1 + x_2$. The red trace represents a trajectory with the initial conditions $x_1(0) = x_2(0) = 0$.Upper left: Linear; Upper right: Truncated Activation; Middle left: Lower Cut-Off; Middle right: Upper and Lower Cut-Offs; Bottom: Logistic LCAs.

8.4.6 Trajectories of the Leaky Competing Accumulators

The trajectories of the LCA models, with different input-ouptut functions considered above, are similar to one another when the LCA is leak dependent. Fig. 8 shows the trajectories of the decision variables $x_1(t), x_2(t)$. These represent the values of the input-current during the course of a single trial. Transforming these using the input-output functions f yield the firing-rates. In order for a decision to be rendered, the firing rates for a neural population selective for one direction of motion (leftward or rightwards) should exceed those of the one selective for the opposite direction. For the Leaky Competing Accumulator model, this corresponds to $f(x_1(t)) > f(x_1(t))$ or vice versa. With the functions considered above if $x_1(t) > x_2(t)$ then $f(x_1(t)) > f(x_1(t))$ and vice versa. Thus it suffices to study only the dynamics of the decision variables $x_1(t), x_2(t)$, representing the dynamic input-currents of the two populations.

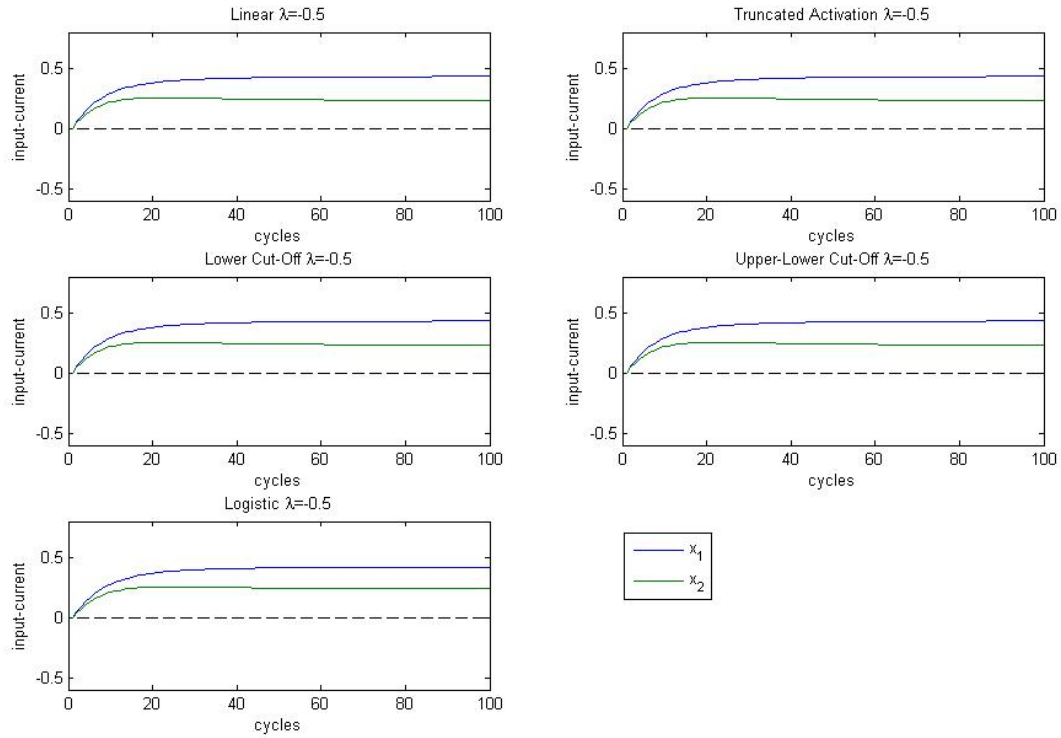

Figure 8: Trajectories of the Leaky Competing Accumulators for a Leak Dependent LCA, i.e. $\lambda = \beta - k < 0$ when Coherence $C \in \left(\frac{\beta-k}{\beta+k} - \frac{\beta-k}{\beta+k}\right)$. Blue and green curves represent the trajectories of the decision variable x_1 and x_2 respectively.

When the motion strength is weak, that is, $C \in \left(\frac{\beta-k}{\beta+k}, -\frac{\beta-k}{\beta+k}\right)$, then the trajectories reach the stable fixed point $(x_1^*, x_2^*) = \left(\frac{\rho_1 k - \rho_2 \beta}{k^2-\beta^2}, \frac{\rho_2 k - \rho_1 \beta}{k^2-\beta^2}\right)$ on the phase plane. The difference between x_1 and x_2 at steady state is very small (Fig. 8). In the presence of noise, it would not be possible to pre-determine which accumulator would win, that

is whether the decision will be left or right. Electrophysiological recordings from the LIP illustrating the time-course of neural firing-rates in the two populations indicate, as discussed in Section 5 (Fig. 5), that the firing rate of the population selective for motion in one direction ramps up while that for the other direction decays or gets inhibited to baseline, as the decision is rendered. However, we observe that this cannot be replicated in our LCA model when it is Leak dependent and small coherences in this particular regime. The winner-take-all-dynamics of one accumulator winning in its evidence accumulation and the other losing, is not possible in this regime. Thus a categorical choice between two competing alternatives is not possible in this case.

For larger coherences, $C \in \left[-\frac{\beta-k}{\beta+k}, 1\right]$, trajectories move to unique, stable a fixed point with $x_1 > x_2$. For all the different types of LCA models considered above, the losing accumulator has a negative input-current (except for the truncated activation function where the firing rates are equal to the input current and are clamped to zero should they fall below it).The firing-rates for one neural population ramp up while those of the other population decay to baseline. Thus, for a sufficiently large strength of the stimulus motion, winner-take-all competition is possible in a leak dependent LCA model and a categorical decision is rendered.

8.5 Balanced LCA: $\beta = k, \lambda = 0$

8.5.1 Linear

When $\lambda = \beta - k = 0$ and f is linear, then Eq. (8.3) has no fixed points when $C \neq 0$. In the noise-free process considered here, trajectories move to the decsion line and move along it. However, when $C = 0$ or equivalently $\rho_1 = \rho_2$, then every point is a fixed point.

8.5.2 Piecewise Linear: Lower Cut-Off

There are stable, fixed points when f is the lower cut-off function. If $C \in (0, 1]$ then the corresponding fixed point is $(x_1, x_2)^* = \left(\frac{\rho_1}{k}, \frac{\rho_2 k - \rho_1 \beta}{k^2}\right)$ where $x_1^* > 0, x_2^* < 0$. Symmetrically, when $C \in [-1, 0)$ then the corresponding fixed point is $(x_1, x_2)^* = \left(\frac{\rho_1 k - \rho_2 \beta}{k^2}, \frac{\rho_2}{k}\right)$ where $x_1^* < 0, x_2^* > 0$. When $C = 0$, every point on the decision line between $\left(0, \frac{\rho_2}{k}\right)$ and $\left(\frac{\rho_1}{k}, 0\right)$ is a fixed point.

8.5.3 Threshold Linear: Upper and Lower Cut-offs

The phase-plane dynamics are similar to that of the Lower Cut-off case when f is the Upper and Lower Cut-off function Eq. (8.21), under the current constraints and parameterization.

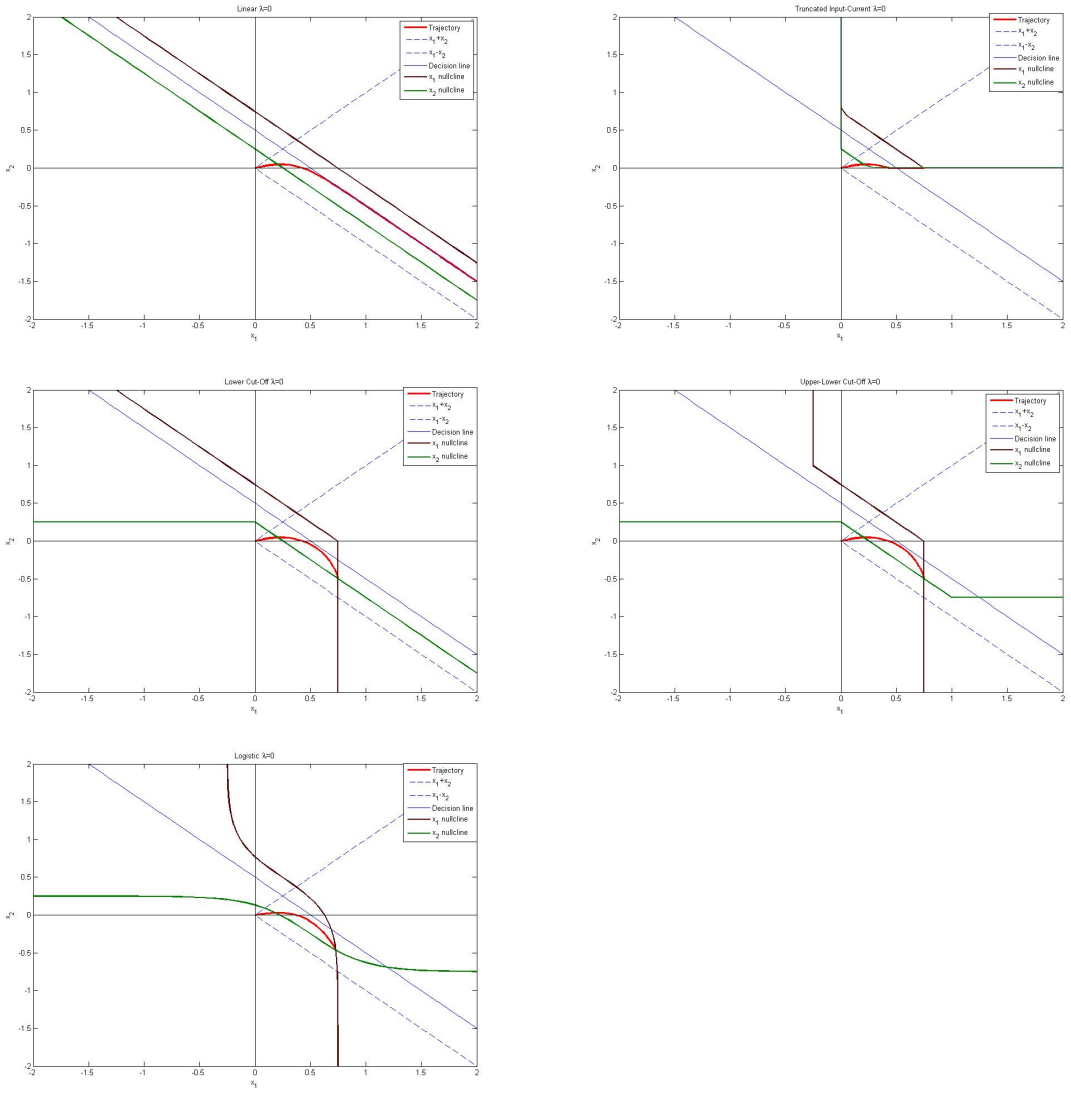

Figure 9: Phase-Plane for the Balanced LCA, i.e.,when $\lambda = \beta - k = 0$ and Coherence $C \in (0, 1]$. Y-axis represents the activity of the decision variable or input-current x_2 and the x-axis represents the activity of the decision variable x_1. The decision line given by Eq. (8.28) is represented by a solid blue line. Brown and green curves correspond to the nullclines for x_1 and x_2 respectively. A point of intersection of the nullclines yields a fixed point. Dashed lines represent the orthogonally transformed coordinates $y_1 = x_1 - x_2$ and $y_2 = x_1 + x_2$. The red trace represents a trajectory with the initial conditions $x_1(0) = x_2(0) = 0$.Upper left: Linear; Upper right: Truncated Activation; Middle left: Lower Cut-Off; Middle right: Upper and Lower Cut-Offs; Bottom: Logistic LCAs.

8.5.4 Trajectories of the Leaky Competing Accumulators

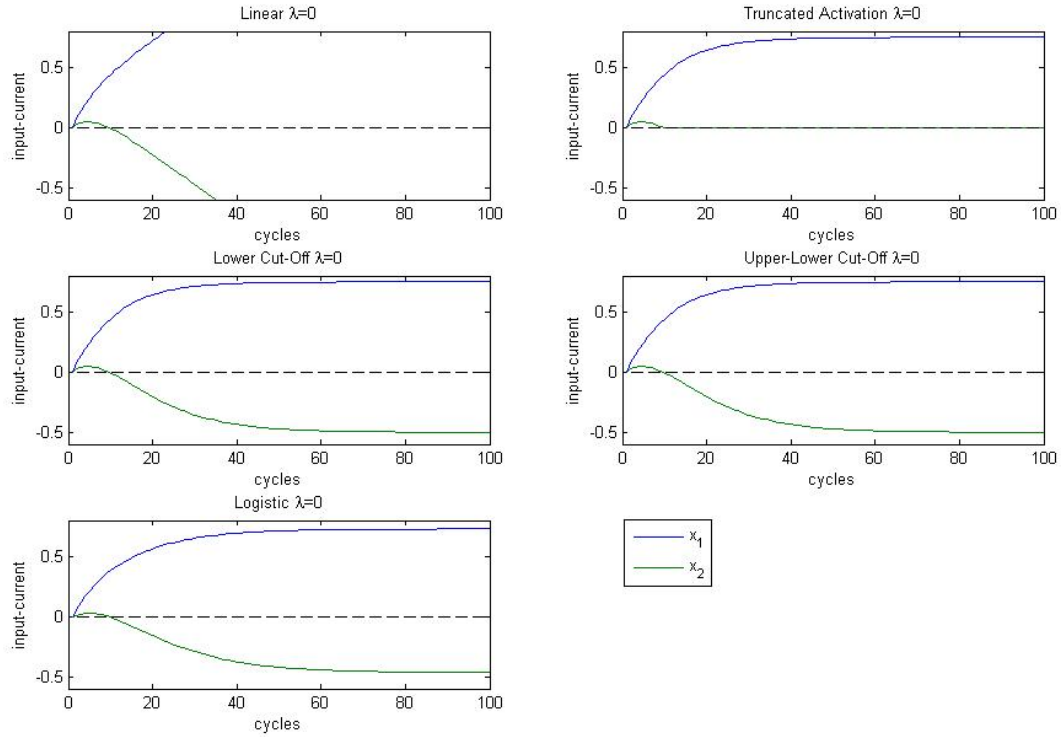

Figure 10: Trajectories of the Leaky Competing Accumulators for a Balanced LCA, i.e. $\lambda = \beta - k = 0$ when Coherence $C \in (0, 1]$. Blue and green curves represent the trajectories of the decision variable x_1 and x_2 respectively.

The trajectories of the LCA models, with different input-ouptut functions considered above, differ from each other when the decay in activation of an accumulator caused by the leak is balanced by the enhancement in activation resulting from the inhibition of the other accumulator, that is, when the LCA is balanced. Fig. 8.5.4 shows the trajectories of the decision variables $x_1(t), x_2(t)$ over the course of a trial.

When the input-output function is linear, the system does not have any fixed points. The input currents or the firing-rates increase or decrease without bound (Fig. 8.5.4, top left panel). On the phase plane, trajectories rapidly approach the decision-line and proceed along it, such that, in the absence of noise, for any coherence favoring a decision unit ($C > 0$ if accumulator 1 is favored and vice versa), firing rates for this continue to ramp up whereas those for the other continues to ramp down, such that a categorical choice is made. The linear model is particularly useful in a Reaction Time task described in Section 4 (Fig. 1 A)or the Free-Response paradigm, where its reduction to a 1-dimensional DDM (8.12) can be used to model Reaction Time distributions [17, 18, 19, 20]. When $C = 0$, there is no drift. Every point on the phase-plane is a fixed point. In that case, noise is required for decision-making to take place.

For the progressively non-linear LCA models, trajectories move along the decision line to reach a fixed point with x_1 winning whenever coherence is positive and vice versa for x_2. The input currents and consequently the firing rates therefore reach steady state and do not increase or decrease without bound (Fig. 8.5.4).

8.6 Inhibition Dependent LCA: $\beta > k, \lambda > 0$

8.6.1 Linear

As in the case for $\beta < k$, solving the system (8.29) yields the unique fixed point $(x_1, x_2)^* = \left(\frac{\rho_1 k - \rho_2 \beta}{k^2 - \beta^2}, \frac{\rho_2 k - \rho_1 \beta}{k^2 - \beta^2}\right)$. Note that this fixed point is always unstable.

Similarly, the unique fixed point can be in one of 3 quadrants, depending on the value of C and hence ρ_1 and ρ_2. We observe that $x_1^*, x_2^* > 0$ when $C \in \left(-\frac{\beta-k}{\beta+k}, \frac{\beta-k}{\beta+k}\right)$. $x_1^* \leq 0, x_2^* > 0$ when $C \in \left[\frac{\beta-k}{\beta+k}, 1\right]$. Finally, $x_1^* > 0, x_2^* \leq 0$ when $C \in \left[-1, -\frac{\beta-k}{\beta+k}\right]$. For our chosen parameter values of $k = 1, \beta = 0.5$, $\frac{\beta-k}{\beta+k} = \frac{1}{5}$.

8.6.2 Piecewise Linear: Lower Cut-Off

When $\beta > k$ and the lower cut-off function Eq. (8.22) is used, then the system given by Eq. (8.3) may, depending on the value of the paramter C have 1, 2 or 3 fixed points. When $C \in \left(-\frac{\beta-k}{\beta+k}, \frac{\beta-k}{\beta+k}\right)$, there are 3 fixed points: $(x_1, x_2)^* = \left(\frac{\rho_1 k - \rho_2 \beta}{k^2 - \beta^2}, \frac{\rho_2 k - \rho_1 \beta}{k^2 - \beta^2}\right)$ corresponds to the fixed point in the positive quadrant. It can be shown that this is a saddle point. When $x_1^* < 0, x_2^* > 0$ then $(x_1, x_2)^* = \left(\frac{\rho_1 k - \rho_2 \beta}{k^2}, \frac{\rho_2}{k}\right)$. Similarly when $x_1^* > 0, x_2^* < 0$ then $(x_1, x_2)^* = \left(\frac{\rho_1}{k}, \frac{\rho_2 k - \rho_1 \beta}{k^2}\right)$. We can show that the latter 2 fixed points are sinks. For $C \in \left(-1, -\frac{\beta-k}{\beta+k}\right) \bigcup \left(\frac{\beta-k}{\beta+k}, 1\right)$ Eq. (8.3) has a stable single fixed point. The fixed point is $(x_1, x_2)^* = \left(\frac{\rho_1 k - \rho_2 \beta}{k^2}, \frac{\rho_2}{k}\right)$ when $C \in \left(-1, -\frac{\beta-k}{\beta+k}\right)$ and is $(x_1, x_2)^* = \left(\frac{\rho_1}{k}, \frac{\rho_2 k - \rho_1 \beta}{k^2}\right)$ when $C \in \left(\frac{\beta-k}{\beta+k}, 1\right)$. For $C = -\frac{\beta-k}{\beta+k}$ there are 2 fixed points, $\left(\frac{\rho_1}{k}, 0\right)$, which is a bifurcation point and the stable fixed point $\left(\frac{\rho_1 k - \rho_2 \beta}{k^2}, \frac{\rho_2}{k}\right)$. Symmetrically when $C = \frac{\beta-k}{\beta+k}$ there the corresponding fixed points are $\left(0, \frac{\rho_2}{k}\right)$ and $\left(\frac{\rho_1}{k}, \frac{\rho_2 k - \rho_1 \beta}{k^2}\right)$.

8.6.3 Threshold Linear: Upper and Lower Cut-Offs

Under the current parameterization and constraints, the phase-plane analysis for the Upper and Lower Cut-Offs case is similar to that of the Lower Cut-Off case above. The solutions for $x_1(t)$ and $x_2(t)$ are therefore similar in both cases.

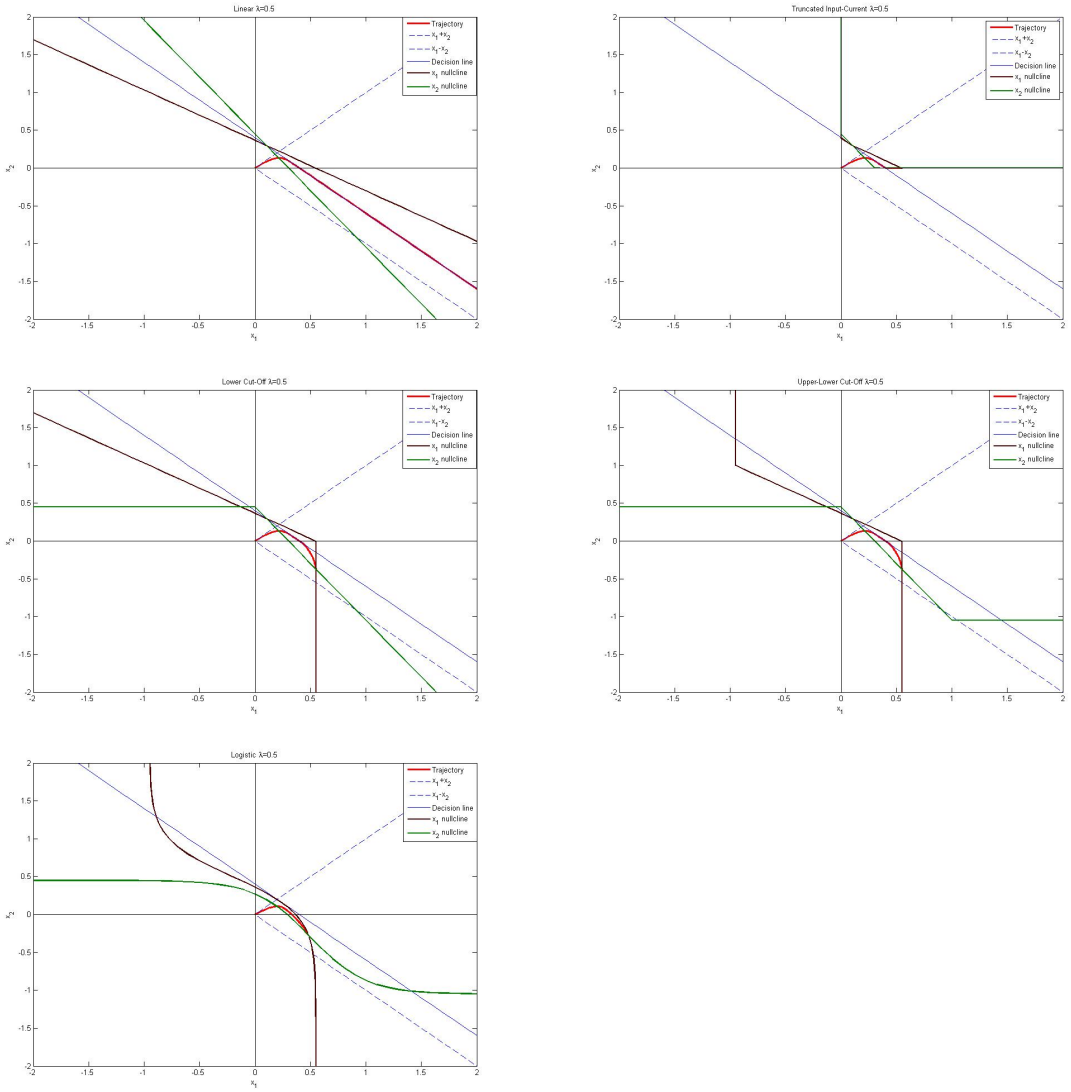

Figure 11: Phase-Plane for the Inhibition Dependent LCA, i.e.,when $\lambda = \beta - k > 0$ and Coherence $C \in \left(\frac{\beta-k}{\beta+k} - \frac{\beta-k}{\beta+k}\right)$.Y-axis represents the activity of the decision variable or input-current x_2 and the x-axis represents the activity of the decision variable x_1. The decision line given by Eq. (8.28) is represented by a solid blue line. Brown and green curves correspond to the nullclines for x_1 and x_2 respectively. A point of intersection of the nullclines yields a fixed point. Dashed lines represent the orthogonally transformed coordinates $y_1 = x_1 - x_2$ and $y_2 = x_1 + x_2$. The red trace represents a trajectory with the initial conditions $x_1(0) = x_2(0) = 0$.Upper left: Linear; Upper right: Truncated Activation; Middle left: Lower Cut-Off; Middle right: Upper and Lower Cut-Offs; Bottom: Logistic LCAs.

8.6.4 Trajectories of the Leaky Competing Accumulators

The trajectories for the different LCA models differ when $\beta > k$. Solutions for x_1 and x_2 diverge rapidly for the linear LCA system since mutual inhibition exceeds leak, and the fixed point is a saddle. A negative input-current value of the losing accumulator boosts that of the winner through the $-\beta x_j$ term since it, in effect involves the subtraction of a large negative term and thus the addition of a large positive term. The losing accumulator on the other hand, becomes more negative owing to the subtraction of a large positive term. This scenario is avoided in the truncated activation case, where the losing accumulator is clamped at zero. Under the current parameterization and constraints, the dynamics for the lower cut-off and upper cut-off cases are similar. Once again, solutions for the winning accumulator are similar for the truncated activation, lower cut-off and upper and lower cut-off conditions, since non-positive input current values of the losing accumulator do not affect the winning accumulator. Obviously, the rate of divergence of the solutions depends on the magnitude of C with faster divergence for larger values of $|C|$.

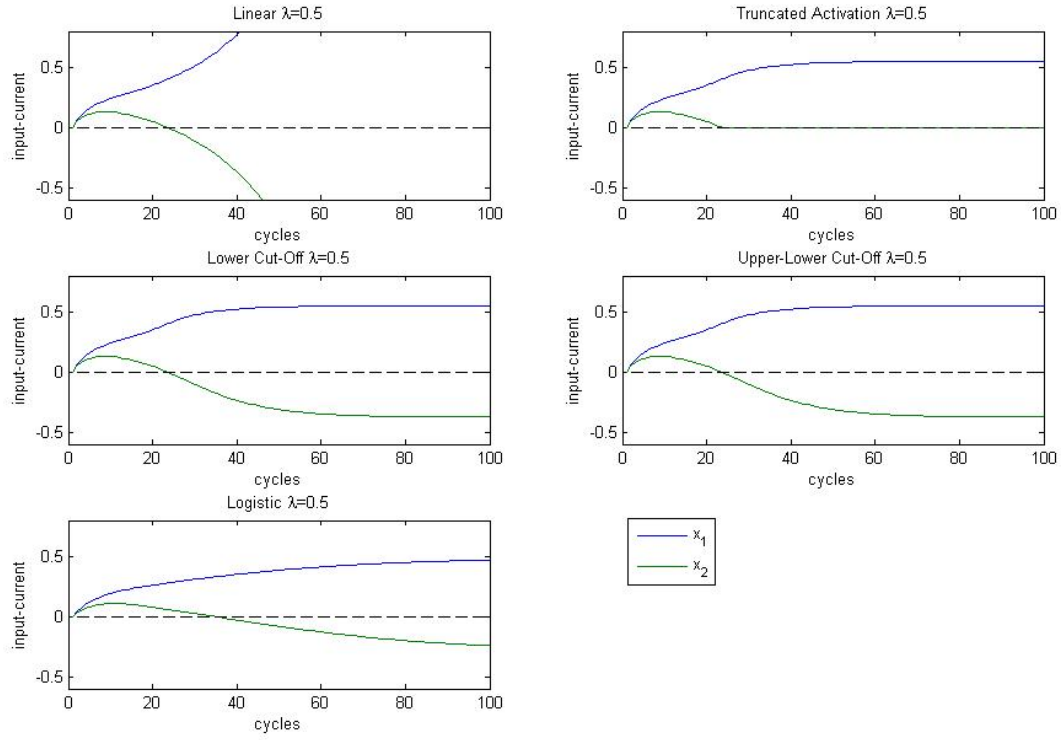

Figure 12: Trajectories of the Leaky Competing Accumulators for an Inhibition Dependent LCA, i.e. $\lambda = \beta - k > 0$ when Coherence $C \in \left(\frac{\beta-k}{\beta+k} - \frac{\beta-k}{\beta+k}\right)$. Blue and green curves represent the trajectories of the decision variable x_1 and x_2 respectively.

The existence of 3 fixed points for the lower cut-off and the upper and lower cut-off functions when coherences are small, that is, $C \in \left(-\frac{\beta-k}{\beta+k}, \frac{\beta-k}{\beta+k}\right)$, with the fixed

point in the positive (first) quadrant being a saddle and those in the second and fourth quadrants being sinks enables winner-take-all-competition between the two decision making accumulators. (Fig. 12). When the trajectories are far from the saddle point, $x_1 = x_2$ and hence the firing rates of the neural populations selective towards the two alternative directions would be equal. Near the saddle point, the two firing-rates split with slow dynamics owing to $\frac{dx_i}{dt}$ being approximately equal to zero. The firing-rates then rapidly diverge as the input current and hence the firing rate of one population ramps up to a stable steady state whereas those of the other poupulation are inhibited to a stable baseline. Since the other fixed points are sinks, depending on whether the coherence is positive or negative, the trajectories are rapidly attracted to them ($x_1^* > x_2^*$ for small positive coherences and vice versa for small negative coherences).

For larger values of $|C|$, the dynamics are similar to the case when the LCA is balanced and coherence is non-zero, except that the firing rates diverge faster.

8.7 Deterministic Leaky Competing Accumulator Model: Summary

In the subsections above, we analyzed the dynamics of the LCA model in the absence of noise, for progressively non-linear input current-output firing-rate functions. We also studied the model's dependence on its parameters, namely the leak k and the inhibition β. Specifically, there existed three types of LCAs: Leak dependent ($\beta < k$), Balanced ($\beta = k$) and Inhibition dependent ($\beta > k$). Analyzing the phase-plane we deduced closed form expressions for fixed points (f.p.s) in terms of the coherence or motion strength C. Our deductions indicate that not only does the coherence influence how fast neural firing rates ramp up or ramp down, but also whether winner-take-all decision-making is possible. In addition, coherence may also determine the number of fixed points possible and the stabitlity of each of those fixed points. For each of the LCAs considered, we found a set of continuous coherence regimes, each generating quantitatively different behaviors on the phase-plane. We noted that the LCAs with a Truncated Activation function are similar to Linear LCAs, except for a clamping of firing-rates to zero should they become negative. The LCA models using a Threshold Linear: Upper and Lower Cut-Off function were similar to those using the Piecewise Linear: Lower Cut-Off functions, except for a set of outer fixed points, which were not attainable under the constraints of the LCA models. We therefore summarize our results for the LCAs employing a Linear and Piecewise Linear: Lower Cut-Off function in Table 8.7.

Note that all three types of LCA models employing a logistic function with a gain or slope of 1, always had a stable fixed point irrespective of the relative magnitudes of Leak and Inhibition. Balanced LCA models with a coherence of 0% have all points on the phase-plane (atleast between two points on a line) becoming fixed points. Specifically, stable fixed points in quadrant II ($x_2 > x_1$) or IV ($x_1 > x_2$) enable winner-take-all dynamics such that one evidence accumulator wins and the other loses and a categorical decision is thereby made. A fixed point which is a saddle

LCA Type	Linear	Lower Cut-Off
Leak Dependent	Unique Stable f.p.	Unique Stable f.p.
Balanced	No f.p. ($C \neq 0$)	Unique Stable f.p. ($C \neq 0$)
Inhibition Dependent	Unique Unstable f.p.	1,2 or 3 f.p.s, either sinks or saddles.

Table 1: Summary of Deterministic LCA models.

causes trajectories to diverge off rapidly from it, enabling fast ramping up of activity for the winning accumulator or neural population and a similarly fast ramping down for the losing population. Such a scenario is obtained for an inhibition dependent LCA model. Our results thus indicate that among the LCA models considered here, an inhibition dependent LCA model represents the most neurally plausible decision-making process.

8.8 Stochastic System

Considering the Leaky Competing Accumulator to be non-deterministic as in Eq. (8.3), we shall compare $p(y_1, t)$ for each of the input-output functions, with the theoretical result in Eq. (8.14). Specifically, we should observe a unimodal distribution with its mean at the unique fixed point when $\beta < k$ and bimodal distribution with modes at the fixed points when $\beta > k$.

8.9 LCA models with Recurrent Self-Excitation: $\alpha \neq 0$

After understanding the dynamics of the relatively mathematically tractable LCA model considered in Eq. (8.3), we shall gradually increase the degree of complexity [10, 28, 4] by considering the complete LCA model described in (8.1). Previously, we had ignored further non-linearities by setting $\alpha = 0$ as in [8, 6], but we shall now include $\alpha > 0$ with the constraint $k = \delta - \alpha$. Crucially, such recurrent self-excitation is important in maintaining spontaneous steady states in biologically realistic models of decision making, such as those discussed below. The reduction in the input current due to the leak k is compensated by the recurrent self-excitation α. The trajectories remain at the spontaneous steady states, enabling the network to display features characteristic of working-memory. We shall compare all results discussed above for system (8.3) with those for system (8.1). We shall also include non-zero base-line activities by varying the shift b for the various input-output functions.

8.10 Gain Modulation

In the input current-output firing rate functions described above, g denoted the slope of the function. Gain modulation refers to changing the amplitude of firing rates for a particular stimulus [25, 26]. In the case of the LCA, this can be achieved by varying the slope or gain g of each of the input-output functions described above [8, 7]. In

particular, previous research [8, 7] has suggested that the release of the neuromodulator norepinephrine from the locus coeruleus has a possible role in modulating such gain. We shall thus examine the effect of varying g on the dynamics of the LCA model by analyzing the phase plane in each case.

Lastly, we shall vary the gain g and/or change the non-linearity of the input-output function within a trial itself and examine the effects of such manipulations on the phase-plane dynamics. We shall then compare simulation results of accuracy and RT distributions with theoretical predictions, in an effort to reconcile simulation results with phase-plane analyses.

9 Gain Modulation in a Non-Linear Neurally Plausible Model of Perceptual Decision Making

Whereas the LCA and OU models can account for behavioral data, time-courses obtained from electrophysiological recordings can be more closely captured by neurally realistic models which use parameters and constraints imported from neurophysiological data. Such models may comprise networks of thousands of spiking neurons interacting with one another, leading to numerous non-linearities and consequent complexities [36]. These models may be reduced through mean-field approaches, which still ensure that a large number of neurophysiological effects are accounted for [40].

Previous work attempting to model the time course of neural firing rates in area LIP have sought to replicate the ramping up of firing rates for the selective neural population accompanied by an inhibition of those for the non-selective population during the stimulus motion period [36, 40, 13] (Fig.5 C). Recent biophysically realistic modeling work has strived to understand the patterns of neural firing over the course of an entire trial, consisting of the fixation, target and stimulus motion periods Fig. (1 A, B), up until a decision is rendered. Firing rates of both the neural populations selective towards their corresponding directions of motion are observed to increase during the target motion period. The targets consist of spots of light placed inside or away from the response fields of the recorded neurons. Neural firing rates for both populations are then observed to decay until they reach a steady firing rate. However, they are also observed to dip together to the same firing level prior at the onset of the dot-motion stimulus. Subsequently, they are observed to diverge as described above. Recent modeling work has been able to accommodate this pattern of firing rate activity by positing that the onset of the stimulus motion switches the primate's attention from the targets to the dot-motion stimulus [39]. Particularly, this is posited to result in a decrease in input currents owing to the encoding of the target, as described in subsection 9.1. We provide a detailed description of this biophysically reaslistic model and its dynamics in that subsection, before modifying and extending it in subsequent subsections.

Modulating the input currents seem a less plausible mechanism considering the targets remain clearly visible on the screen (Fig.1 A, B) even during the stimulus motion period. Gain modulation offers and alternative yet neurally plausible mechanism for explaining the mutual effects of attention and decision making. We posit that such an interaction between attention and decision-making, manifest in the gain modulation of single neurons in the LIP, enables the pattern of neural firing activity observed in electrophysiological experiments. We discuss this mechanism in the subsection 9.4. We perform phase plane analyses, similar to our analyses for the LCA models, but for a deterministic biophysically realistic model, when neural gain is kept constant or modulated dynamically over the course of a trial.

We deduce that an attention mediated increase in gain (slope of the input-output function) for excitatory populations only prevents winner-take-all-competition, which is necessary for categorical perceptual decision-making. We explain how the modu-

lation of both excitatory and inhibitory neural populations serves as a mechanism for not only enabling categorical choice, but also flexible decision-making. Such a neurally plausible mechanism accounts for firing rate data observed in both Reaction Time and Fixed Viewing Duration decision making tasks.

9.1 Reduced Two-Variable Biophysically Realistic Model

The biophysically realistic model of Wang [36] comprised 2000 spiking neurons and 7200 dynamical equations. The decision network consisted of two neural populations selective towards the two alternative directions of motion, left and right, a non-selective population, selective towards neither direction of motion and a population of inhibitory interneurons. The two selective populations receive inputs from the MT and each population possesses recurrent self-excitatory connections. Applying a mean-field approach, this spiking neuron model can be reduced to a four-variable model. Employing a simplified input-output function [40], linearizing the input-ouput function for inhibitory interneurons and assuming constant firing activity of the non-selective population, the network is further reduced to a three-variable model. If all fast variables are assumed to reach steady state early, the effects of AMPA synapses on the selective populations can be neglected and the network becomes the reduced two-variable (Fig. 13) that we shall henceforth discuss.

The function relating the input synaptic current I_i to the output firing rate r_i of the two selective neural pools is given by

$$r_i = f(I_i) = \frac{aI_i - b}{1 - \exp\left[-d(aI_i - b)\right]} \tag{9.1}$$

where i is either L(representing leftward) or R(denoting rightward), $a = 270$ Hz/nA, $b = 108$ Hz and $d = 0.154$s. Then the two-variable model is given by the system

$$\begin{aligned} I_{L,tot} &= J_{LL}S_L - J_{LR}S_R + I_{motion,L} + I_{target} + I_{noise,L} \\ I_{R,tot} &= J_{RR}S_R - J_{RL}S_L + I_{motion,R} + I_{target} + I_{noise,R} \end{aligned} \tag{9.2}$$

where S_L and S_R are the dynamic variables of the system, representing synaptic gating variables for neurons selective for leftward and rightward directions of motion. The synaptic couplings $J_{LL} = J_{RR} = 0.3725$ nA represent recurrent self-excitation and $J_{LR} = J_{RL} = 0.1137$ nA represent mutual inhibition. $I_{motion,i}$ represents the input from the dot-motion stimulus. The current I_{target} represents the encoded targets, which are spots of light placed inside or away from the response fields of the neurons in a population. The neural populations receive noisy background synaptic inputs, which are modeled by a mean input I_0 and a fluctuating white noise component filtered by a synaptic time constant τ_{noise}.

$$\tau_{noise}\frac{dI_{noise,i}(t)}{dt} = -\left(I_{noise,i}(t) - I_0\right) + \sigma_{noise}\sqrt{\tau_{noise}}N(0,1) \tag{9.3}$$

where $\sigma_{noise} = 0.009$ nA and $\tau_{noise} = 2$ ms. We further assume that the network dynamics is dominated by S_i, which have slower time constants than the firing rates

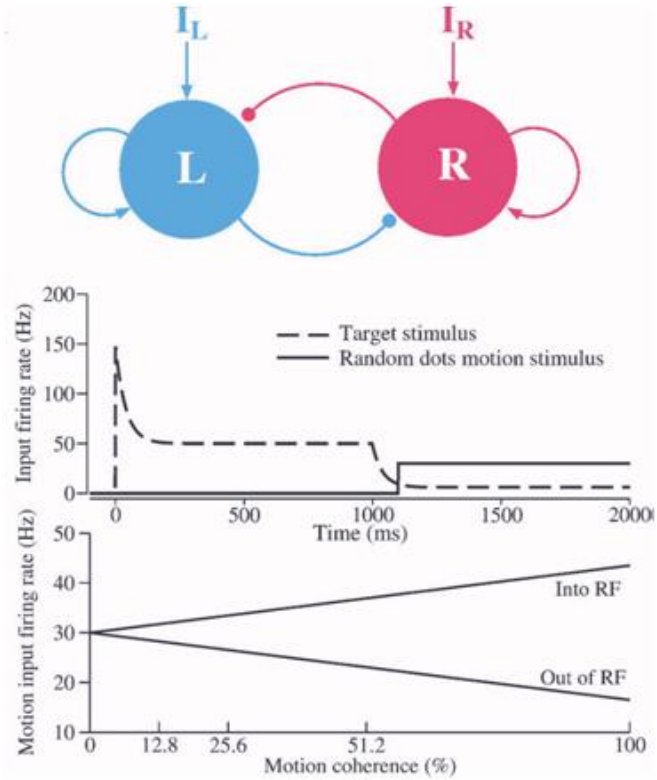

Figure 13: A reduced biophysically realistic decision- making network model. (A) The network consists of two units, representing two competing neural pools selective for leftward and rightward motion, respectively. Each is endowed with strong self-excitatory recurrent coupling (sharp arrowheads). Cross-coupling between the two units is effectively inhibitory (circular arrowheads), through a shared inhibitory neural pool which is not explicitly represented in this reduced model. I_L (I_R) encompasses the external inputs from motion-selective (MT) neurons, target-sensitive neurons, and background neurons. (B) Inputs to the decision units within a trial consist of both target stimulus inputs (dashed line) and motion stimulus from the random-dots (bold line; shown here with zero motion coherence). According to the model, the target inputs are reduced when the random-dot motion appears because attention is directed to the motion. (C) The directional input comes from MT cells, whose firing rates depend linearly on motion coherence. Coherent motion toward (opposite) the response field, RF, increases (decreases) the cell's output firing rate. Reproduced from [39].

r_i. That is, we assume that r_i have already attained their steady-states while the S_i have not. Then the dynamics of S_i are governed by

$$\frac{dS_i}{dt} = -\frac{S_i}{\tau_S} + (1 - S_i)\gamma f(I_i) \tag{9.4}$$

where $\gamma = 0.641$ and $\tau_s = 60$ ms. Firing rates of neurons in the MT, selective for a particular direction of motion, increase roughly proportional to the coherence or motion strength when the motion is in the preferred direction for the neuron. Thus the input current encoding stimulus motion, which is relayed to the LIP decision neurons is given by

$$I_{motion,i} = J_A \mu_0 \left(1 + \kappa \frac{c}{100}\right) \tag{9.5}$$

where $\kappa = 0.45$ is a stimulus-signal gain parameter, $J_A = 1.1 \times 10^-3$ nA/Hz, $\mu_0 = 30$ Hz and $c \in [-100, 100]$. A transient decay of the firing rates of MT neurons during stimulus presentation is neglected for the sake of simplicity.

The input current due to the encoded target can be modeled as

$$I_{target} = \begin{cases} 0 & t < t_{target} \\ J_A \left(50 + 100 \exp\left[-\frac{(t - t_{target})}{\tau_{ad}}\right]\right), & t_{target} \leq t \leq t_{motion} \\ J_A \left(6 + 44 \exp\left[-\frac{(t - t_{motion})}{\tau_{ad}}\right]\right), & t \geq t_{motion} \end{cases} \tag{9.6}$$

where t_{target} and t_{motion} are the onset times of the targets and dot-motion stimuli, respectively. This input current has a short-time adaptation, represented by a decay with a time constant of $\tau_{ad} = 40$ ms.When the non-linear Input Current-Output Firing-Rate function given by Eq.(9.1), this yields high firing-rates when the targets are first presented. The firing rates decay with a short-time adaptation, with the input current due to the target reaching a steady level at $J_A \times 50$ nA. During the stimulus motion period, the input current due to the target again decays, from $J_A \times 50$ nA to an eventual steady state of $J_A \times 6$ nA. This manipulation is explained as resulting from a shift in attention from the targets to the stimulus motion. In the next subsection, we argue that it is this dip in target input current, together with the onset of stimulus that enables the network to make a categorical decision.

9.2 Phase-Plane Analysis of Reduced Two-Variable Biophysical Model with Attention Mediated Changes in Target Input Currents

Using the non-linear Input Current-Output Firing-Rate function given by Eq.(9.1), we can analyze the phase-plane during different periods over the course of a trial.

The steady states of the deterministic form of system (9.4) can be obtained by solving for the nullclines

$$-\frac{S_i}{\tau_S} + (1 - S_i)\gamma f(I_i) = 0 \tag{9.7}$$

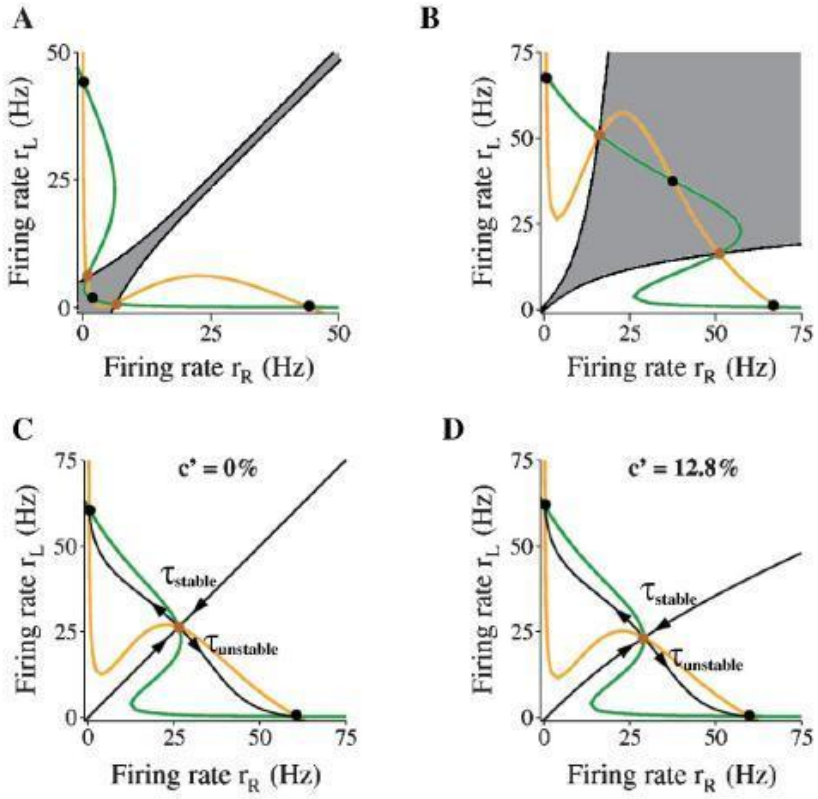

Figure 14: Reconfiguration of the decision network during different epochs of a trial. Phase planes show the nullclines of the population firing rates selective to leftward (r_L) and rightward (r_R) motion, represented by orange and green lines. Black (brown) filled circles are the stable (unstable) steady-states of the network. Black lines with direction of arrows toward and away from the saddle point yield the stable and unstable manifolds of the saddle point. Gray region is the basin of attraction of the spontaneous state in (A), or that of the symmetrical stable state in (B). (A)Without visual target nor motion stimulus input to decision network. (B) With target input only. Steady-states after adaptation. (C) With both (reduced) saccadic target input and motion stimulus of zero coherence. (D) With both (reduced) saccade target input and motion stimulus of 12.8% coherence. Reproduced from [39].

In the absence of any target or motion-stimulus inputs, the network possesses three stable steady states, represented by black dots in Fig. 9.2A. These include the spontaneous, symmetrical steady state with low firing rates $r_L = r_R$, and the assymetric, persistent steady states. The co-existence of these steady states allows the network to exhibit working-memory capabilities. A transient stimulus switches the network from the resting state to one of the two persistent steady states. Since the persistent, off-diagonal steady states are stable, the decision is self-sustained, and retained in working memory. The stable manifolds for the saddle points of the network during this epoch separate the phase plane into basins of attraction. The grey region represents the basin of attraction for the symmetric steady state with a low firing rate. When the target appears, both selective populations receive a high input current, which pushes the network to now have a high symmetrical, stable, steady state with $r_L = r_R \approx 37.5$ Hz (Fig. 9.2B). The large basin of attraction ensures that winner-take-all-competition is reduced and the network remains in this symmetrical, high firing-rate condition during target presentation. The reduction in input current due to the target owing to a shift in attention from the target to the input stimulus, together with the onset of the stimulus reconfigures the network such that there are only two stable steady states: the asymetrical, off-diagonal, persistent steady states. The symmetric steady state now becomes a saddle, allowing winner-take-all competition and decision-making to take place. For a coherence of 0 %, the basins of attraction for both persistent states are equal (Fig. 9.2C). For coherences favoring the leftward direction, the basin of attraction for r_L is much larger than that for r_R (Fig. 9.2D). In the presence of noise, correct decisions involve sample paths remaining within this basin.

9.3 Firing Rates of the Two Selective Populations

The target and motion stimulus input currents and the consequent firing rates of the two neural pools are shown in Fig. 13. The firing rates of both pools increase rapidly at target presentation, decaying with the passage of time. After stimulus presentation, attention is shifted from the targets to the stimulus motion, leading to a dip in the firing rates of both pools. The firing rates then separate as observed by the ramping up to threshold for one pool and simultaneous inhibition to baseline of the other.

When we average over many trials or consider the system to be noise-free and thus deterministic, we observe that this splitting of the firing rates for the two pools occurs at a firing rates less than the maximum firing rate attained when only the target is on. This corresponds to observations (Fig. 15) from most electrophysiological experiments using the dot-motion task [22, 29, 13]. However, in some experiments employing the Reaction Time task [22], this splitting was observed at firing rates greater than the steady state firing rate attained when only the target is presented (Fig. 5 C).

Performing the phase plane analysis above considering symmetric inputs $I_L = I_R$, we can vary μ_0 in Eq. (9.5) to get the bifurcation diagram, $r_i = f\left(I_i(S_{i,j})\right)$. We shall obtain a mushroom shaped diagram, with a saddle corresponding to the time

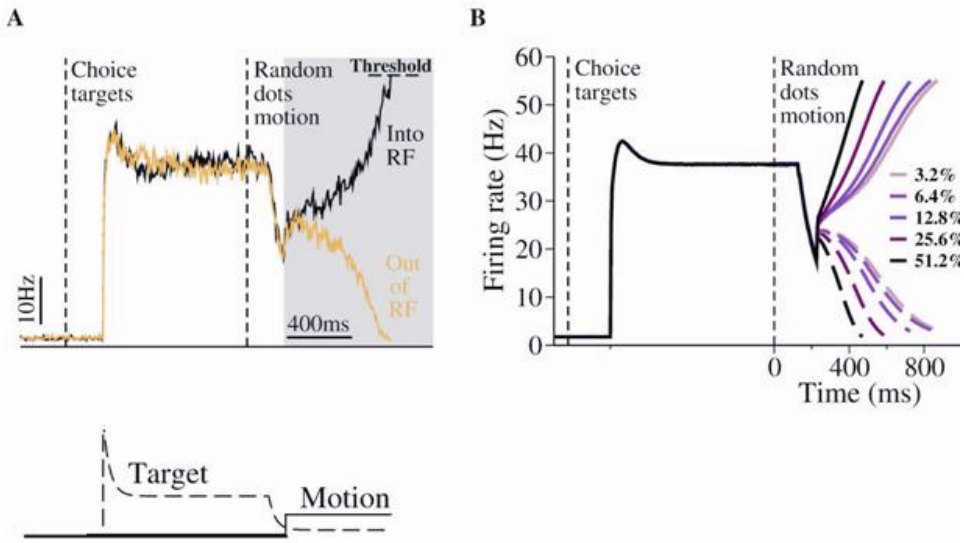

Figure 15: Neural dynamics of the decision network model. (A) Top: A sample trial with zero motion coherence. During target presentation, both neural pools (black and orange lines) achieve a relatively high steady state firing rate, similar to the observation of LIP neurons. During motion stimulus presentation (gray box), the firing rates of the two neural pools first increase together, then diverge over time, one ramping up whereas the other ramping down, resulting in a categorical choice (the decision bound is fixed at 55 Hz). Bottom: inputs. The target input represents static visual stimulus inputs with adaptation, as observed in experiments. The motion stimulus resembles the output firing rates of MT neurons. Note that in order to reproduce the dip immediately in neural activity immediately after motion stimulus onset, the target input is assumed to decrease (due to divided attention) after the motion stimulus onset but before the motion signals reach the LIP neurons. (B) Trial-averaged neural activities of the two neural pools with five motion coherence levels. Solid curves: winning population; dashed curves: losing population. Time courses of neural activity are aligned at the time of motion onset. Note slower ramping activity at a lower motion coherence. Only correct trials are shown. Reproduced from [39].

and firing rate at which this splitting occurs There are also stable fixed points when $t_{target} \leq t \leq t_{motion}$ and when $t < t_{target}$. Owing to the monotonicity of the unstable manifold, $r_{L/R}(t_{target}) > r_{L/R}(t_{splitting})$, corresponding to the observation in most electrophysiological experiments. In order to account for the results in from some experiments employing the Reaction Time task [22], we would want $r_{L/R}(t_{target}) < r_{L/R}(t_{splitting})$. This however, cannot be achieved with the present model. We posit that modulating the gain of the input-out functions provides a mechanism for achieving this.

In addition, the fact that the two targets stay on during the course of a trial lends credence to the notion that the input currents due to the targets should remain at their steady state value of $J_A \times 50$ nA instead of further decreasing when the motion stimulus is present. Wong et al [39] explained this dip in input current as representing an attentional shift from the target to the dot-motion stimulus. However, as we demonstrate in subsequent subsections, the dip in neural firing rates can be achieved

by changing the gain of both the selective populations and the inhibitory populations that were explicitly present in the spiking neuron model of Wang [36] but implicitly respresented through the synaptic coupling constants J_{LL}, J_{RR}, J_{LR} and J_{RL}. In the following subsection, we discuss such attention mediated gain modulation as a putative mechanism affecting decision-making.

9.4 Attention Mediated Gain Modulation

As discussed in Subsection 9.3 the fact that the two choice targets remain on, clearly visible on the screen even during the presentation of the dot-motion stimulus indicates that the current due to the target I_{target} should remain constant at its previous steady state value over the course of the motion stimulus and not decay further. Accordingly we alter Eq. (9.6) to

$$I_{target} = \begin{cases} 0 & t < t_{target} \\ J_A \left(50 + 100 \exp\left[-\frac{(t-t_{target})}{\tau_{ad}}\right]\right), & t \geq t_{target} \end{cases} \tag{9.8}$$

When the stimulus motion comes on, the net current due to the target and motion increases. Whereas it was possible to reconfigure the decision-making network to exhibit winner-take-all-competition involved in making a categorical choice when I_{target} was given by Eq. (9.6), using Eq. (9.8) necessitates an alternative mechanism for simulating both the dip in firing rates and winner-take-all-dynamics. Gain modulation offers one such mechanism.

9.4.1 Attention Mediated Gain Modulation in the LIP during Perceptual Decision-Making

In order to incorporate the effects of attention mediated gain modulation of the selective neural populations in the LIP, Eq. (9.1) in our reduced two-variable can be approximated as

$$r_i = f(I_i) = \frac{g_E a I_i - b}{1 - \exp\left[-d(g_E a I_i - b)\right]} \tag{9.9}$$

where as before, i is either L(representing leftward) or R(denoting rightward), $a = 270$ Hz/nA, $b = 108$ Hz and $d = 0.154$s. g_E represents the slope or *gain* of the input current-output firing rate transfer function (Fig. 16), and $g_E = 1$ for the dynamics described in previous sections.

Gain modulation of the selective populations can be accomplished in several ways, the simplest of which is to use a larger value of g but using $g(t) = g$, for all t. A larger value of $g(t) = g$ yields unrealistically high firing rates during the target period and thus such a manipulation cannot be neurally implemented.

Alternatively, we could modulate the gain at the onset of the motion stimulus, according to

$$g_E = \begin{cases} g_{E_1}, & t < t_{motion} \\ g_{E_2}, & t \geq t_{motion} \end{cases} \tag{9.10}$$

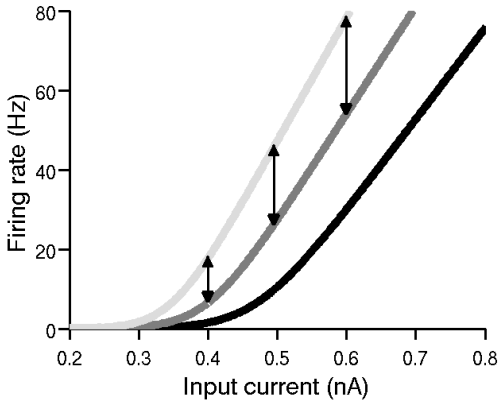

Figure 16: Gain modulation of input current-output firing rate transfer function

Varying the gain from $g_{E_1} = 1$ to $g_{E_2} > g_{E_1}$ at motion stimulus onset, enables higher firing rates than previously achieved during the motion stimulus period. However, as we discuss below this also reduces winner-take-all competition, preventing categorical decision-making .

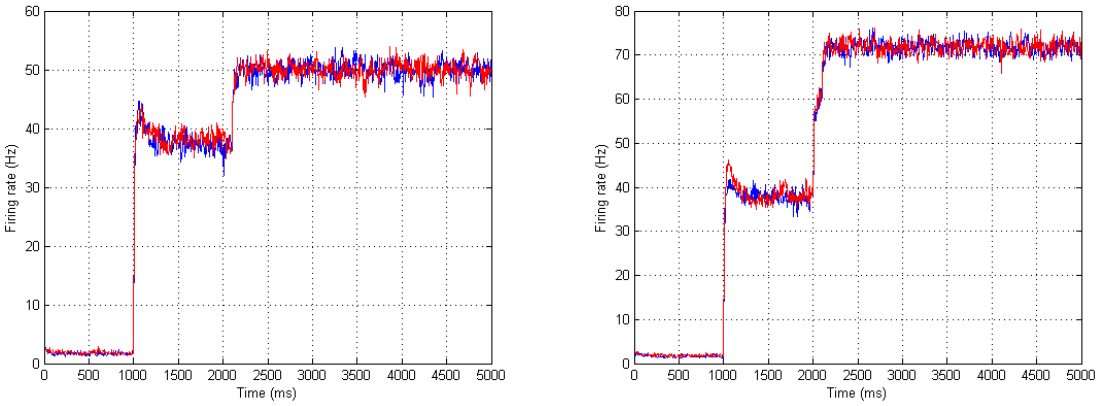

Figure 17: Time courses of firing rates for two selective populations with gain modulated according to Eq. (9.10), with $g_{E_2} = 1$ (left) and 1.1 (right), respectively. Note that the although the firing rates are larger, winner-take-all-competition cannot be achieved as g_{E_2} is increased from 1.

Thus, in order to ensure neurally realistic winner-take-all-competition, increasing the gain of the direction selective, decision-making population should be accompanied by increasing the gain of the inhibitory interneuron population originally present in the spiking neuron model of Wang [36]. In the reduced, two-variable model these are absorbed into the synaptic coupling constants: the recurrent self-excitations $J_{LL} = J_{RR}$, and the mutual inhibitions $J_{LR} = J_{RL}$. Let $J_{LL} = J_{RR} = \alpha_1$ and

$J_{LR} = J_{RL} = \alpha_2$. Then we can derive (not shown here) that,

$$\begin{aligned} \alpha_1 &= k_{w_+} - \frac{k_1 c_I}{1 + k_2 c_I} \\ \alpha_2 &= k_{w_-} - \frac{k_3 c_I}{1 + k_2 c_I} \end{aligned} \tag{9.11}$$

Then

$$\alpha_1 - \alpha_2 = k_w^{'} - \frac{k^{'} c_I}{1 + k_2 c_I}, \tag{9.12}$$

where all k_ws are constants. We thus observe that the effective synaptic couplings depend on the gain c_I of inhibitory neurons.

9.5 Phase-Plane Analysis with Attention-Mediated Gain Modulation of Excitatory and Inhibitory Neural Populations

In order to find the fixed points of the reduced two-variable system, we solve the nullclines Eq. (9.7). As discussed in subsection 9.2, in the absence of any target or motion-stimulus inputs, the network possesses three stable steady states, (Fig. 9.5, Upper Left panel). These include the spontaneous, symmetrical steady state with low firing rates $r_L = r_R$, and the asymetric, persistent steady states. The co-existence of these steady states allows the network to exhibit working-memory capabilities as a transient stimulus can switch the network from the resting state to one of the two persistent steady states. The stable manifolds (separatrices) for the saddle points of the network during this epoch separate the phase plane into basins of attraction. The grey region represents the basin of attraction for the symmetric steady state with a low firing rate. When the target appears, both selective populations receive a high input current, which pushes the network to now have a high symmetrical, stable, steady state with $r_L = r_R \approx 37.5$ Hz (Fig. 9.5, Upper Right panel). The large basin of attraction ensures that winner-take-all-competition is reduced and the network remains in this symmetrical, high firing-rate condition during target presentation.

Consider coherence to be 0%, both selective populations receive equal input $I_L = I_R$. Thus $I_{motion,L} = I_{motion,R}$. In the deterministic case, both populations receive a constant background excitatory input I_{0_E}. The symmetrical steady state that plays the crucial role in decision-making shall have $S_1^* = S_2^*$.

$$\begin{aligned} -\frac{S^*}{\tau_S} + (1 - S^*)\gamma f(I) &= 0 \\ -\frac{S^*}{\tau_S} + (1 - S^*)\gamma f(J_{LL}S^* - J_{LR}S^* + I_{motion} + I_{target} + I_{0_E}) &= 0 \\ -\frac{S^*}{\tau_S} + (1 - S^*)\gamma f\left((\alpha_1 - \alpha_2)S^* + I_{ext}\right) &= 0 \end{aligned}$$

where α_1 and α_2 are given by Eq. (9.11) and their difference depends on the inhibitory interneuronal gain given by Eq. (9.12).

Thus we observe that the symmetrical steady state depends both on the gain of excitatory, selective populations g_{E_2} and that of the inhibitory interneuronal populations c_I. Implementing the input current-output firing-rate function given in Eq. (9.1) restricts the firing rates from being too high, and is thus more neurally realistic. Varying the gain g_{E_2} for selective,excitatory populations at the onset of the motion stimulus and allowing the system to reach steady-state, we can analyze the phase plane. We consider the case of both populations receiving equal inputs, with $c = 0\%$. The following results were based on analysis conducted using the XPPAUT software.

When the motion stimulus is presented and the input current due to the target remains at a steady state value, instead of decaying further, the network remains stable if we increase only excitatory gain $g_{E_2} \geq 1$ (Fig. 9.5, Lower Left panel). Thus, as we increase or keep the gain of the excitatory, selective populations constant without simultaneously increasing the gain of the inhibitory populations, the network loses its winner-take-all features and categorical decision-making does not take. If we sufficiently increase the gains of both excitatory and inhibitory populations simultaneoulsy, then the network reaches a saddle point. Trajectories therefore approach this saddle and then are attracted toward one of the persitent, off-diagonal fixed points. Thus firing-rates shall rise together and then diverge as those for one selective population ramps up while those for the other are inhibited down to baseline. We have henced deduced that attention mediated gain modulation of both excitatory, selective neurons and inhibitory interneurons in the LIP enables decision-making in two alternative forced choice tasks. In addition, such a mechanism allows the splitting of firing rates during the stimulus motion period to be at a higher level than the firing-rates when only the target is present, as observed in Reaction Time experiments [22].

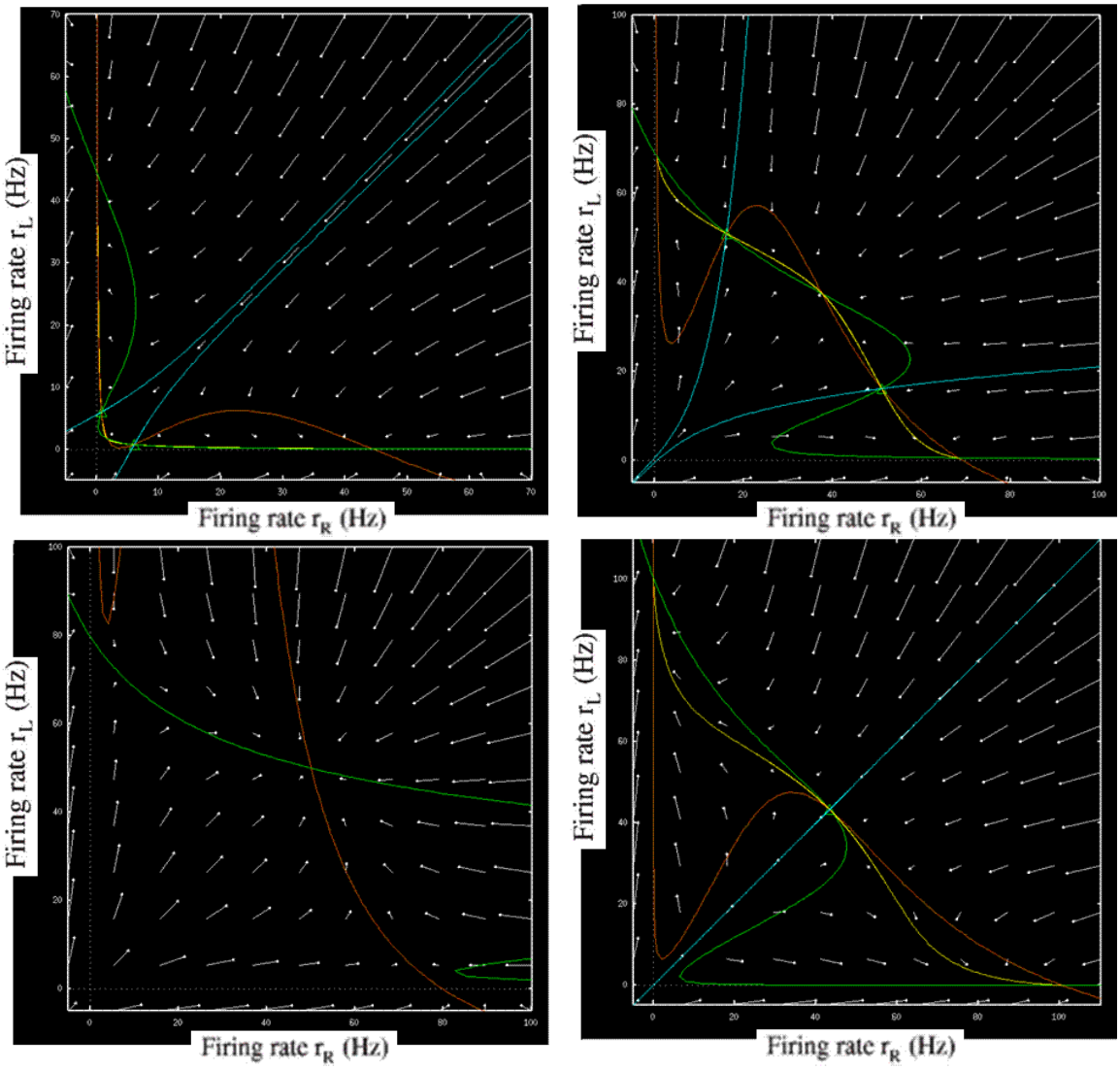

Figure 18: Phase planes show the nullclines of the population firing rates selective to leftward (r_L) and rightward (r_R) motion, represented by orange and green lines. Points of intersection of the nullclines yield the steady-states of the network. Blue curves represent stable manifolds while yellow curves represent unstable manifolds of a fixed point. Blue curves separate the phase plane into basins of attractions. Direction fields dictate the trajectories of solutions starting from different intial conditions. Upper Left panel: Without visual target nor motion stimulus input to decision network. Upper Right panel: With target input only. Steady-states after adaptation. Lower Left panel: Stimulus period: Steady target current, only increasing the excitatory gain according to Eq. (9.10), with $g_{E_2} \geq 1$, without changing the inhibitory gain. Lower Right panel: Stimulus period: Increasing both g_{E_2} and c_I, $g_{E_2} = 1.49$ and $c_I = 2.30$.

Although we deduced this dependence on both excitatory and inhibitory neurons in the case where coherence was 0 %, it also holds when the two selective populations receive unequal inputs, that is motion is predominantly towards one direction. For instance with coherence is 12.8 % towards the left, we observe larger basin of attraction for the neural population selective towards leftward saccades (Fig. 9.5). In the presence of noise, this enables mor choices to be correct, that is, decisions should correctly identify the direction of motion to be the left.

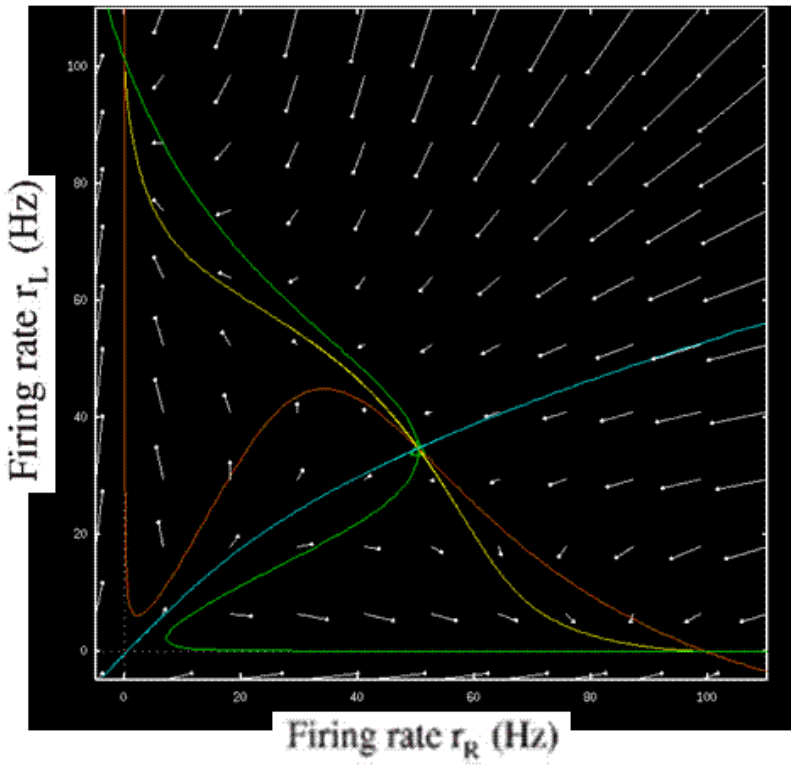

Figure 19: Phase-Plane shows the nullclines of the population firing rates selective to leftward (r_L) and rightward (r_R) motion, represented by orange and green lines. Points of intersection of the nullclines yield the steady-states of the network. Blue curve represents a stable manifold while yellow curve represents an unstable manifold of a fixed point. Blue curves separate the Phase-Plane into basins of attractions. Direction fields dictate the trajectories of solutions starting from different intial conditions. Stimulus Period with steady input current due to the target. Coherence 12.8 %, increasing both g_{E_2} and c_I.

Keeping μ_0 and c_I constant, we can study the effect of varying g_{E_2} on the dynamics of the network by exploring the bifurcation diagram, considering g_{E_2} to be the relevant parameter 9.5. We observe that when $g_{E_2} \leq 0.835$ only a single, stable fixed point exists. When $0.835 < g_{E_2} < 0.93$ then the two asymetrical stable persistent steady states remain along with two unstable fixed points. At $g_{E_2} = 0.84$, a bifurcation occurs, such that the network transitions to enable decision-making between two alternatives. We obtain a symmetrical, saddle point along with the two persistent states. This saddle branch is lower than the upper stable branch during the target period. Another bifurcation occurs at $g_{E_2} = 0.94$, such that the saddle becomes a

stable fixed point and two unstable steady states are also obtained, reconfiguring the network such that it is equivalent to the case when only the target is present, and winner-take-all-competition along with categorical decision-making is prevented.

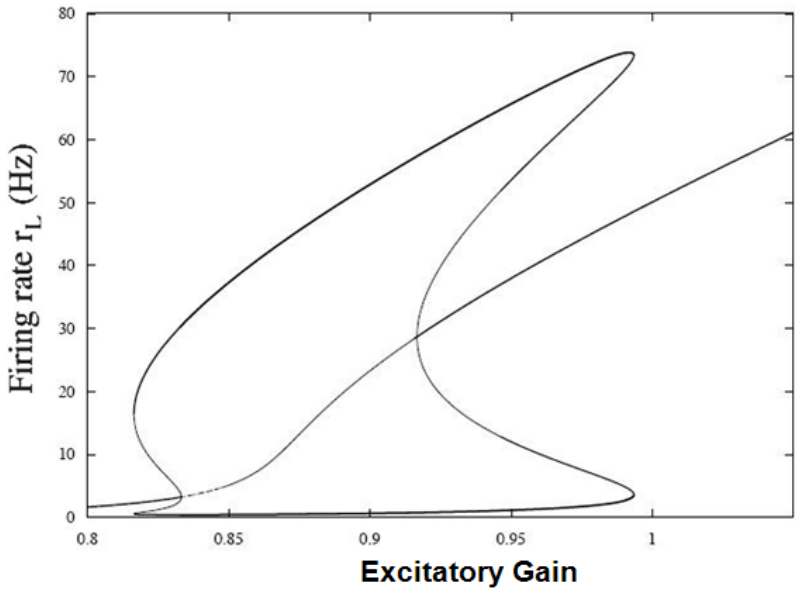

Figure 20: Bifurcation diagram with g_{E_2} as the parameter, keeping $c_I = 1$ and $\mu_0 = 26$ Hz fixed. Dark lines represent stable branches whereas light curves represent unstable branches.

In similar fashion, we can investigate the bifurcation diagram by varying the gain of the inhibitory interneuron population c_I, which affects the synaptic coupling constants, while keeping $g_{E_2} = 1$ and $\mu_0 = 26$ Hz fixed (Fig. 9.5). Decreasing the gain of inhibitory interneurons during the stimulus period without simultaneously decreasing the gain of excitatory neurons reconfigures the network such that it attains a symmetrical steady state and decision-making is not possible.

We have thus shown that attention mediated gain modulation of neurons in the LIP serves as a putative, neurally plausible mechanism for enabling winner-take-all-dynamics and categorical decision-making between two competing alternatives. Specifically, we have demonstrated that such gain modulation is an alternative to a reduction in input currents due to choice targets resulting from a shift in attention at stimulus motion onset, even when the choice targets remain clearly visible on the screen. Gain modulation directly results in the modulation of firing rates and not the direct modulation of input currents. Furthermore, both the gains of excitatory, selective neurons and inhibitory interneurons must be modulated simultaneously during the motion stimulus period to enable categorical decision-making. Gain modulation thus gates the appropriate neural population such that a correct decision is made.Such modulation can also replicate the dip in firing rates previously attributed to a shift in attention from the target to the motion stimulus (Fig. 22).

Keeping the strength of the inputs from the MT constant, that is, considering $\mu_0 = 26Hz$, we shall search for the ratios of excitatory and inhibitory gains that

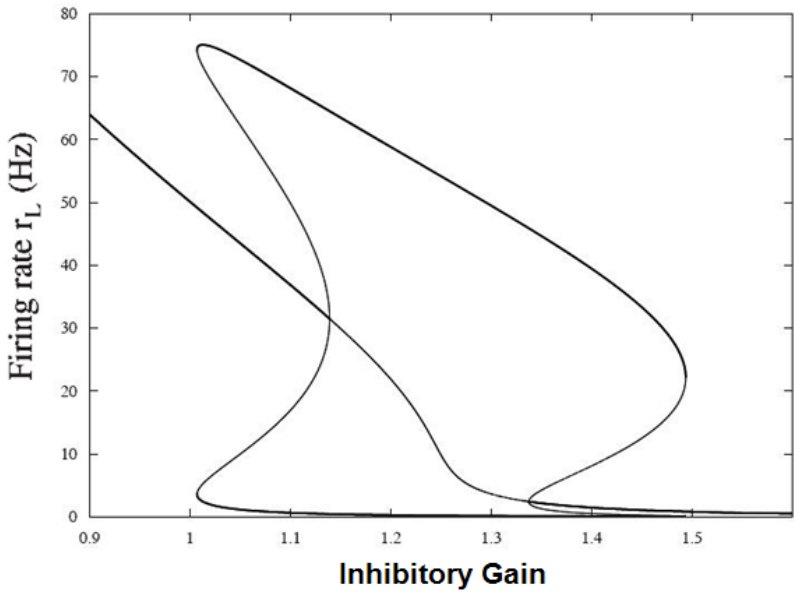

Figure 21: Bifurcation diagram with c_I as the parameter, keeping $g_{E_2} = 1$ and $\mu_0 = 26$ Hz fixed. Dark lines represent stable branches whereas light curves represent unstable branches.

capture experimental findings from both Reaction Time and Fixed Viewing Duration TAFCs. Similar to previous work on LCA models [8], we shall attempt to find optimal gain schedules for both excitatory and inhibitory populations taken together.

Similar to the analyses above, we shall explore the bifurcation diagram with μ_0 as the parameter. Subsequently, we are particularly interested in the g_{E_2} vs μ_0, c_I vs μ_0 and g_{E_2} vs c_I phase diagrams. The stability patterns observed on these phase diagrams will guide our manipulations of g_{E2} and c_I at the onset of motion stimulus. We shall modulate these gains for the excitatory selective and inhibitory interneuronal populations and explore the Phase-Plane as before. Crucially, we shall attempt to ensure winner-take-all-competition is maintained, and a saddle point exists at firing rates $r_{L/R}(t_{splitting}) > r_{L/R}(t_{target})$, the stable symmetrical steady state firing rate during the target period. We shall then investigate the 3 dimensional bifurcation diagram: $r_{L/R} = f(I_{L,R}, g)$ and $r_{L/R} = f(I_{L,R}, c_I)$ to gain a clearer understanding of the dynamics of this model.

In future work, we shall extend the results obtained here to study the specific dynamics of decision-making in fixed viewing duration tasks. We also seek to understand how a possible waxing and waning gain influences behavioral performance by exploring RT distributions obtained from conduting several simulations with noisy trials. Thus far, we have contrasted steady, constant gain during motion stimulus presentation with a decaying gain, with no significant differences between them (Fig.22).

Of particular interest is how reward biases decision-making in the LIP, and whether attention, for instance through gain modulatory mechanisms, plays a role in such reward-based decision-making. The gating of the correct decision by fast atten-

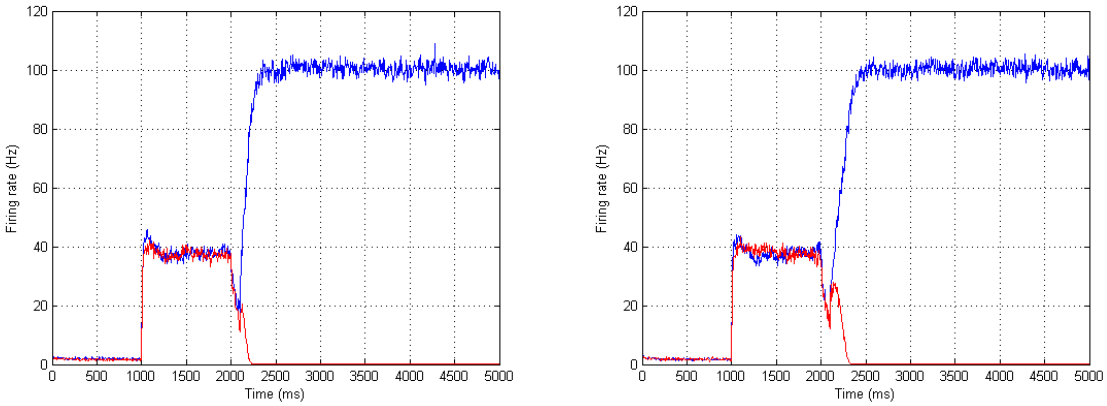

Figure 22: Time courses of firing rates for two selective populations when increasing both g_{E_2} and c_I. Left: Excitatory gain $g_{E_2} = 1.49$ and inhibitory gain $c_I = 2.30$ are kept constant. Right: Excitatory and inhibitory gains decay.

tion mediated gain modulation indicates that such mechanisms may be influential in a task-switching paradigm, where they may enable a decision-making network to switch to the pertinent task or stimuli.Finally, we shall extend the results obtained here to other study other gain modulatory effects on decision making, such as those that are context-dependent, or task-dependent [25, 26, 27, 24, 21].

10 Conclusion

Although previous research in behavioral economics has delineated the criteria for optimal decision-making, such research has focused more on optimal outcomes than on the neural mechanisms underlying decision-making. We are interested more in the dynamics of the decision process and its possible implementations in the neural circuitry. Recent studies in neuroscience have made progress in identifying the neural systems associated with such processes [5, 22, 29], particularly for perceptual decision-making tasks. Specifically, we explored perceptual decision in Two-Alternative Forced-Choice (TAFC) tasks where a subject must choose one of two alternatives on each trial. Electrophysiological recordings in the Middle Temporal (MT) and Lateral Intraparietal etal (LIP) cortices of awake, behaving primates performing a dot-motion discrimination task have revealed qualitatively distinguishable firing rate patterns of neurons in the two areas. Whereas firing-rates for MT neurons are noisy and depend only on the coherence, those for the LIP neurons exhibit a ramping up to a decision threshold for neurons selective for the appropriate direction of motion, accompanied by a simultaneous ramping down for neurons selective for the opposite direction of motion. The mathematical models we explored sought to account for these electrophysiological findings while positing mechanisms underlying decision-making that can be experimentally evaluated.

We employed an abstract, Leaky Competing Accumulator (LCA) model [32, 8], studying the effects of non-linearities, relative magnitudes of the parameters and coherence on the decision rendered. In particular, we considered the LCA to be Leak dependent, Balanced or Inhibition dependent. Performing a phase-plane analysis to find the fixed points of our system, we deduced closed form expressions for fixed points in terms of the coherence. Our deductions suggest that not only does the coherence determine how fast neural firing-rates ramp up or ramp down, but in addition, whether winner-take-all decision-making resulting in a categorical choice is possible. We derived that coherence also determine the number of fixed points possible and the stabitlity of each of those fixed points. For each of the LCAs considered, we derived a set of continuous coherence regimes, each predicting quantitatively different behaviors on the phase-plane. We showed that stable fixed points in Quadrant II and IV enable winner-take-all decision-making, as do saddle points. Specifically, the presence of a saddle enables rapid divergence of the trajectories for the two decision units used to model the two neural populations. This occurs in the case of an Inhibition dependent LCA. Since this corresponds best to the electrophysiological data, we posit that an inhibition dependent LCA is the most neurally plausible among the LCA models that we considered.

In order to model the time-course of neural firing-rates more accurately, we considered a two-variable biophysically realistic model of perceptual-decision making [39], which had previously been reduced from a network of several thousand spiking neurons [40]. Recent research attempting to model the time-course over the duration of an entire trial had posited that the onset of the motion stimulus after the target

period caused a decrease in input currents encoded for the target by LIP neurons. An analysis of the phase-plane had revealed that this reduced input current together with the onset of the stimulus caused the decision network to switch from a stable steady state to a saddle, enabling categorical choice [39]. However, considering the fact that the target remains clearly visible on the screen for the entire duration of a trial, it is unlikely that the input currents due to the target should decay. We offer the attention mediated gain modulation of LIP neurons [21] as an alternative and more neuarally plausible mechanism for perceptual decision-making.

Gain modulation refers to changing the slope of the input current-output firing rate (transfer) function for a neuron or a population of neurons [25, 26, 27, 24, 21, 7, 8]. We performed a phase-plane analysis similar to that for the LCA models study the behavior of the network during different epochs in a trial. Specifically, we obtained a high symmetrical stable state when only the target was present, corresponding to the firing-rates of both populations remaining at a high value. Increasing the gain of only excitatory neurons selective towards the two directions of motion at the onset of the motion stimulus, made the network attain a higher stable fixed point. This prevented the winner-take-all dynamics that is required for a categorical choice. Decreasing the gain permitted such dynamics, but the saddle now obtained corresponded to firing-rates that were too low to be realistic. We derived that the fixed points also depended on the gain of inhibitory interneuronal populations, which had been incorporated into the synaptic coupling coefficients in the reduced two-variable model. We noted that changing the gain of both excitatory and inhibitory interneurons reconfigured the network such that it possessed a saddle point corresponding to neurally realistic firing-rates. Divergence of the firing-rates took place near the saddle, enabling winner-take-all dynamics and ensuring categorical decision-making.

Considered together, our modeling effort reflects a mathematical analysis based, dynamical systems approach to understanding the mechanisms underlying decision-making. Both our models constitute processes that merit basic study independent of applications. In addition, according to our mathematical analyses, they generate predictions that can be empirically tested.

References

[1] Barnard, G.A. (1946). Sequential tests in industrial statistics. *Journal of Royal Statistical Society Supplement*,8, 1-26.

[2] Bogacz R, Brown ET, Moehlis J, Hu P, Holmes P and Cohen JD (2006). The physics of optimal decision making: A formal analysis of models of performance in two-alternative forced choice tasks. *Psychological Review*, 113, 700-765.

[3] Bogacz, R., and Cohen, J.D. (2004). Parameterization of connectionist models. *Behavioral Research Methods, Instruments, and Computers*, 36, 732-741.

[4] Botvinick, M., Braver, T.S., Barch, D., Carter, C., and Cohen, J.D. (2001). Conflict monitoring and cognitive control. *Psychological Review*,108, 625-652.

[5] Britten, K.H., Shadlen, M.N., Newsome, W.T., and Movshon, J.A. (1993). Responses of neurons in macaque MT to stochastic motion signals. *Visual Neuroscience*, 10, 1157-1169.

[6] Brown, E., and Holmes, P. (2001). Modeling a simple choice task: stochastic dynamics of mutually inhibitory neural groups. *Stochastics and Dynamics*, 1, 159-191.

[7] Brown, E., Gilzenrat, M., and Cohen, J.D. (2004). The locus coeruleus, adaptive gain, and the optimization of simple decision tasks. Technical Report: 04-02, Center for the Study of Mind, Brain, and Behavior, Princeton University.

[8] Brown, E., Gao, J., Holmes, P., Bogacz, R., Gilzenrat, M., and Cohen J.D. (2005). Simple networks that optimize decisions. *International Journal of Bifurcations and Chaos*,15, 803-826.

[9] Busemeyer, J.R., and Townsend, J.T. (1993). Decision field theory: A dynamic-cognitive approach to decision making in uncertain environment.*Psychological Review*, 100, 432-459.

[10] Cho, R.Y., Nystrom, L.E., Brown, E., Jones, A.D., Braver, T.S., Holmes, P.J., and Cohen, J.D. (2002). Mechanisms underlying dependencies of performance on stimulus history in a two-alternative forced-choice task. *Cognitive Affective and Behavioral Neuroscience*, 2, 283-299.

[11] Ditterich, J. (2006). Stochastic models of decisions about motion direction: Behavior and Physiology. *Neural Networks*, 19, 981-1012.

[12] Ermentrout, G.B. (1994). Reduction of conductance-based models with slow synapses to neural nets. *Neural Computation*, 6, 679-695.

[13] Gold, J.I., and Shadlen, M.N. (2001). Neural computations that underlie decisions about sensory stimuli. *Trends in Cognitive Sciences*, 5, 10-16.

[14] Kahneman, D., and Tversky, A. (1984). Choices, values, and frames. *American Psychologist*, 39, 341-350.

[15] Mazurek, M., Roitman, Ditterich, J., and Shadlen, M. (2003). A role for neural integrators in perceptual decision making. *Cerebral Cortex*, 13, 12571269.

[16] Neyman. J., and Pearson, E.S. (1933). On the problem of the most efficient tests of statistical hypotheses. *Philosophical Transactions of the Royal Society London, Series A*, 231, 289-337.

[17] Ratcliff, R. (1980). A note on modelling accumulation of information when the rate of accumulation changes over time. *Journal of Mathematical Psychology*, 21, 178-184.

[18] Ratcliff, R. (1985). Theoretical interpretations of the speed and accuracy of positive and negative responses. *Psychological Review*, 92, 212-225.

[19] Ratcliff, R., and Rouder, J.N. (1998). Modeling response times for two-choice decisions. *Psychological Science*, 9, 347-356.

[20] Ratcliff, R., and Rouder, J.N. (2000). A diffusion model account of masking in two-choice letter identification. *Journal of Experimental Psychology: Human Perception and Performance*, 26, 127-140.

[21] Reynolds J.H., Chelazzi L. (2004). Attentional modulation of visual processing. *Annual Reviews of Neuroscience*, 27,611-47.

[22] Roitman, J.D., and Shadlen, M.N. (2002). Response of neurons in the lateral intraparietal area during a combined visual discrimination reaction time task. *Journal of Neuroscience*, 22, 9475-9489.

[23] Rumelhart, D.E., J.L. McClelland, and the PDP Research Group, *Parallel Distributed Processing: Explorations in the Microstructure of Cognition. Vol. I: Foundations*. 1986, (Cambridge, MA: MIT Press).

[24] Salinas E, Abbott L.F. (2002). A model of multiplicative neural responses in parietal cortex. *Proceedings of the National Academy of Sciences, U S A*. 93(21),11956-61.

[25] Salinas E. and Thier P. (2000). Gain modulation: a major computational principle of the central nervous system. *Neuron*, 27(1),15-21.

[26] Salinas E. and Sejnowski T.J. (2001). Gain modulation in the central nervous system: where behavior, neurophysiology, and computation meet. *Neuroscientist*.7,430-40.

[27] Salinas E. (2004). Fast remapping of sensory stimuli onto motor actions on the basis of contextual modulation. *Journal of Neuroscience*, 24(5),1113-8.

[28] Simen, P., Cohen J.D. and Holmes P. (2006). Rapid decision threshold modulation by reward rate in a neural network. *Neural Networks*, 19, 1013-1026.

[29] Shadlen, M.N., and Newsome, W.T. (2001). Neural basis of a perceptual decision in the parietal cortex (area LIP) of the rhesus monkey. *Journal of Neurophysiology*, 86, 1916-1936

[30] Smith, P. L., and Ratcliff, R. (2004). Psychology and neurobiology of simple decisions. *Trends in Neurosciences*, 27, 161168.

[31] Strogatz, S. H. (2001). *Nonlinear dynamics and chaos: with applications to physics,biology, chemistry and engineering.*(Cambridge, MA, Perseus Books Group).

[32] Usher, M., and McClelland, J.L. (2001). On the time course of perceptual choice: the leaky competing accumulator model. *Psychological Review*, 108, 550-592.

[33] Vickers, D. (1970). Evidence for an accumulator model of psychophysical discrimination. *Ergonomics*, 13, 37-58.

[34] Wald, A. (1947). Sequential Analysis. New York: Wiley.

[35] Wald, A., and Wolfowitz, J. (1948). Optimum character of the sequential probability ratio test. *Annals of Mathematical Statistics*, 19, 326-339.

[36] Wang, X.-J. (2002). Probabilistic decision making by slow reverberation in cortical circuits. *Neuron*, 36, 1-20.

[37] Wilson, H. R., and Cowan, J. D. (1972). Excitatory and inhibitory interactions in localized populations of model neurons. *Biophysical Journal*, 12, 1-24.

[38] Wilson, H.R. and Cowan, J.D. (1973). A Mathematical Theory of the Functional Dynamics of Cortical and Thalamic Nervous Tissue. *Kybernetik*,13, 55-80.

[39] Wong, K-F, Huk, A.C., Shadlen, M.N. and Wang, X-J (2007). *Frontiers in Computational Neuroscience*, 1, 1-11.

[40] Wong, K-F and Wang, X-J (2006). A recurrent network mechanism of time integration in perceptual decisions, *Journal of Neuroscience*, 26,1314-1328.